30 nM using Lipofectamine RNAiMAX (Invitrogen) in accordance with the manufacturer's instructions. Target sequences of the siRNAs were: occludin (5'-GCAAGAUCACUAUGAGACA-3'), SR-BI (5'-GAGCUU-UGGCCUUGGUCUA-3'), CD81 (5'-CUGUGAUCAUGAUCUUCGA-3'), CHC (5'-CUAGCUUUGCACAGUUUAA-3'), Dyn2 (5'-CCCUCA-AGGAGGCGCUCAA-3'), Cav1 (5'-CCCUAAACACCUCAACGAU-3'), flotillin-1 (5'-CCUAUGACAUCGAGGUCAA-3'), Arf6 (5'-CAGUU-CUUGGUAAAGUCCU-3'), CtBP1 (5'-GACUCGACGCUGUGCC-ACA-3') and PAK1 (5'-GCAUCAAUUCCUGAAGAUU-3'). Target sequences of the siRNAs for claudin-1, PI4K and scrambled negative control were as described previously (Suzuki et al., 2013).

Immunoblotting. Cells were washed with PBS and incubated with passive lysis buffer (Promega). Lysates were sonicated for 10 min and added to the same volume of 2 × SDS-PAGE sample buffer. Protein samples were boiled for 10 min, separated by SDS-PAGE and then transferred to PVDF membranes (Merck Millipore). After blocking, membranes were probed with primary antibodies, followed by incubation with peroxidase-conjugated secondary antibody. Antigen–antibody complexes were visualized using an enhanced chemiluminescence detection system (SuperSignal West Pico Chemiluminescent Substrate; Thermo Scientific) in accordance with the manufacturer's protocols.

Flow cytometry. Cultured cells detached by treatment with trypsin were incubated with anti-CD81 antibody or anti-mouse IgG antibody for 1 h at 4 °C. After being washed with PBS containing 0.1 % BSA, cells were incubated with an Alexa Fluor 488-conjugated anti-mouse secondary antibody (Invitrogen) for 1 h at 4 °C, washed repeatedly and resuspended in PBS. Analyses were performed using a FACSCalibur system (Becton Dickinson).

Reagents and antibodies. Bafilomycin A1 was obtained from Wako Pure Chemical Industries. Alexa Fluor 488-conjugated transferrin was obtained from Invitrogen. For immunoblotting, anti-SR-BI (NB400-104; Novus Biologicals), anti-occludin (71-1500; Invitrogen), anti-claudin-1 (51-9000; Invitrogen), anti-Dyn2 (ab3457; Abcam), anti-Cav1 (N-20; Santa Cruz Biotechnology), anti-flotillin (H-104; Santa Cruz Biotechnology), anti-Arf6 (ab77581; Abcam) and anti-PAK1 (2602; Cell Signaling Technology) rabbit polyclonal antibodies; anti-CD81 (JS-81; BD Biosciences), anti-β-actin (AC-15; Sigma-Aldrich), anti-CHC (23; BD Biosciences), anti-GRAF1 (SAB1400439; Sigma-Aldrich) and anti-glyceraldehyde 3-phosphate dehydrogenase (6C5; Merck Millipore) mouse mAb; and anti-CtBP1 goat polyclonal antibody (C-17; Santa Cruz Biotechnology) were used. For immunofluorescence staining, anti-CHC mAb (X22) and anti-HA rat polyclonal antibody (3F10) were obtained from Thermo Scientific and Roche Applied Science, respectively. Anti-NS5A antibody was a rabbit polyclonal antibody against synthetic peptides. Alexa Fluor 488- or 555-labelled secondary antibodies were obtained from Invitrogen.

DNA transfection. Cell monolayers were transfected with plasmid DNA using TransIT-LT1 transfection reagent (Mirus) in accordance with the manufacturer's instructions.

Treatment of cells with bafilomycin A1 and cell viability. Cells were preincubated with various concentrations of bafilomycin A1 for 60 min at 37 °C. Preincubated cells were then infected with HCVtcp. Cells treated with 0.1 % DMSO were used as controls. Cell viability was analysed by the Cell Titre-Glo Luminescent Cell Viability Assay (Promega).

Uptake of transferrin. Cells were grown on glass coverslips. After cells were transfected with HA-tagged Dyn2 expression plasmids, Alexa Fluor 488-conjugated transferrin at 20 µg ml^{-1} was added and incubated for 30 min. Cells were washed with PBS and fixed in 4 % paraformaldehyde.

Immunofluorescence analysis. Huh7.5.1 and Huh-7 cells were fixed with 4 % paraformaldehyde in PBS for 30 min, and were then blocked and permeabilized with 0.3 % Triton X-100 in a non-fat milk solution (Block Ace; Snow Brand Milk Products) for 60 min at room temperature. Samples were then incubated with anti-CHC, anti-Dyn2, anti-Cav1, anti-NS5A or anti-HA for 60 min at room temperature, washed three times with PBS, and then incubated with secondary antibodies for 60 min at room temperature. Finally, samples were washed three times with PBS, rinsed briefly in double-distilled H$_2$O and mounted with DAPI mounting medium. The signal was analysed using a Leica TCS SPE confocal microscope.

Luciferase assay. For quantification of FLuc activity in HCVtcp-infected cells, cells were lysed with passive lysis buffer (Promega) at 72 h post-infection. FLuc activity of the cells was determined using a luciferase assay system (Promega). For quantification of GLuc activity in supernatants of HCVtcp-infected cells, the Renilla Luciferase Assay System (Promega) was used. All luciferase assays were performed at least in triplicate.

Quantification of HCV core protein. HCV core protein was quantified using a highly sensitive enzyme immunoassay (Lumipulse G1200; Fujirebio) in accordance with the manufacturer's instructions.

ACKNOWLEDGEMENTS

REFERENCES

Acosta, E. G., Castilla, V. & Damonte, E. B. (2008). Functional entry of dengue virus into Aedes albopictus mosquito cells is dependent on clathrin-mediated endocytosis. J Gen Virol 89, 474–484.

Acosta, E. G., Castilla, V. & Damonte, E. B. (2009). Alternative infectious entry pathways for dengue virus serotypes into mammalian cells. Cell Microbiol 11, 1533–1549.

Akazawa, D., Date, T., Morikawa, K., Murayama, A., Omi, N., Takahashi, H., Nakamura, N., Ishii, K., Suzuki, T. & other authors (2008). Characterization of infectious hepatitis C virus from liver-derived cell lines. Biochem Biophys Res Commun 377, 747–751.

Bartosch, B., Vitelli, A., Granier, C., Goujon, C., Dubuisson, J., Pascale, S., Scarselli, E., Cortese, R., Nicosia, A. & Cosset, F. L. (2003). Cell entry of hepatitis C virus requires a set of co-receptors that include the CD81 tetraspanin and the SR-B1 scavenger receptor. J Bio Chem 278, 41624–41630.

Benedicto, I., Molina-Jimenez, F., Bartosch, B., Cosset, F. L., Lavillette, D., Prieto, J., Moreno-Otero, R., Valenzuela-Fernandez, A., Aldabe, R., Lopez-Cabrera, M. & Majano, P. L. (2009). The tight junction-associated protein occludin is required for a postbinding step in hepatitis C virus entry and infection. J Virol 83, 8012–8020.

Blanchard, E., Belouzard, S., Goueslain, L., Wakita, T., Dubuisson, J., Wychowski, C. & Rouillé, Y. (2006). Hepatitis C virus entry depends on clathrin-mediated endocytosis. J Virol 80, 6964–6972.

Blight, K. J., McKeating, J. A. & Rice, C. M. (2002). Highly permissive cell lines for subgenomic and genomic hepatitis C virus RNA replication. J Virol 76, 13001–13014.

Codran, A., Royer, C., Jaeck, D., Bastien-Valle, M., Baumert, T. F., Kieny, M. P., Pereira, C. A. & Martin, J. P. (2006). Entry of hepatitis C

virus pseudotypes into primary human hepatocytes by clathrin-dependent endocytosis. *J Gen Virol* 87, 2583–2593.

Coller, K. E., Berger, K. L., Heaton, N. S., Cooper, J. D., Yoon, R. & Randall, G. (2009). RNA interference and single particle tracking analysis of hepatitis C virus endocytosis. *PLoS Pathog* 5, e1000702.

Damke, H., Baba, T., van der Bliek, A. M. & Schmid, S. L. (1995). Clathrin-independent pinocytosis is induced in cells overexpressing a temperature-sensitive mutant of dynamin. *J Cell Biol* 131, 69–80.

Damm, E. M., Pelkmans, L., Kartenbeck, J., Mezzacasa, A., Kurzchalia, T. & Helenius, A. (2005). Clathrin- and caveolin-1-independent endocytosis: entry of simian virus 40 into cells devoid of caveolae. *J Cell Biol* 168, 477–488.

Evans, M. J., von Hahn, T., Tscherne, D. M., Syder, A. J., Panis, M., Wolk, B., Hatziioannou, T., McKeating, J. A., Bieniasz, P. D. & Rice, C. M. (2007). Claudin-1 is a hepatitis C virus co-receptor required for a late step in entry. *Nature* 446, 801–805.

Grove, J. & Marsh, M. (2011). The cell biology of receptor-mediated virus entry. *J Cell Biol* 195, 1071–1082.

Grove, J., Nielsen, S., Zhong, J., Bassendine, M. F., Drummer, H. E., Balfe, P. & McKeating, J. A. (2008). Identification of a residue in hepatitis C virus E2 glycoprotein that determines scavenger receptor BI and CD81 receptor dependency and sensitivity to neutralizing antibodies. *J Virol* 82, 12020–12029.

Helle, F., Vieyres, G., Elkrief, L., Popescu, C.-I., Wychowski, C., Descamps, V., Castelain, S., Roingeard, P., Duverlie, G. & Dubuisson, J. (2010). Role of N-linked glycans in the functions of hepatitis C virus envelope proteins incorporated into infectious virions. *J Virol* 84, 11905–11915.

Hoofnagle, J. H. (2002). Course and outcome of hepatitis C. *Hepatology* 36 (Suppl 1), S21–S29.

Kambara, H., Fukuhara, T., Shiokawa, M., Ono, C., Ohara, Y., Kamitani, W. & Matsuura, Y. (2012). Establishment of a novel permissive cell line for the propagation of hepatitis C virus by expression of microRNA miR122. *J Virol* 86, 1382–1393.

Kataoka, C., Kaname, Y., Taguwa, S., Abe, T., Fukuhara, T., Tani, H., Moriishi, K. & Matsuura, Y. (2012). Baculovirus GP64-mediated entry into mammalian cells. *J Virol* 86, 2610–2620.

Kato, N., Mori, K., Abe, K., Dansako, H., Kuroki, M., Ariumi, Y., Wakita, T. & Ikeda, M. (2009). Efficient replication systems for hepatitis C virus using a new human hepatoma cell line. *Virus Res* 146, 41–50.

Liu, S., Yang, W., Shen, L., Turner, J. R., Coyne, C. B. & Wang, T. (2009). Tight junction proteins claudin-1 and occludin control hepatitis C virus entry and are downregulated during infection to prevent superinfection. *J Virol* 83, 2011–2014.

Lupberger, J., Zeisel, M. B., Xiao, F., Thumann, C., Fofana, I., Zona, L., Davis, C., Mee, C. J., Turek, M. & other authors (2011). EGFR and EphA2 are host factors for hepatitis C virus entry and possible targets for antiviral therapy. *Nat Med* 17, 589–595.

Marsh, M. & Helenius, A. (2006). Virus entry: open sesame. *Cell* 124, 729–740.

Matlin, K. S., Reggio, H., Helenius, A. & Simons, K. (1981). Infectious entry pathway of influenza virus in a canine kidney cell line. *J Cell Biol* 91, 601–613.

McKeating, J. A., Zhang, L. Q., Logvinoff, C., Flint, M., Zhang, J., Yu, J., Butera, D., Ho, D. D., Dustin, L. B., Rice, C. M. & Balfe, P. (2004). Diverse hepatitis C virus glycoproteins mediate viral infection in a CD81-dependent manner. *Journal of virology* 78, 8496–8505.

Meertens, L., Bertaux, C. & Dragic, T. (2006). Hepatitis C virus entry requires a critical postinternalization step and delivery to early endosomes via clathrin-coated vesicles. *J Virol* 80, 11571–11578.

Mercer, J., Schelhaas, M. & Helenius, A. (2010). Virus entry by endocytosis. *Annu Rev Biochem* 79, 803–833.

Miaczynska, M. & Stenmark, H. (2008). Mechanisms and functions of endocytosis. *J Cell Biol* 180, 7–11.

Mosso, C., Galván-Mendoza, I. J., Ludert, J. E. & del Angel, R. M. (2008). Endocytic pathway followed by dengue virus to infect the mosquito cell line C6/36 HT. *Virology* 378, 193–199.

Norkin, L. C., Anderson, H. A., Wolfrom, S. A. & Oppenheim, A. (2002). Caveolar endocytosis of simian virus 40 is followed by brefeldin A-sensitive transport to the endoplasmic reticulum, where the virus disassembles. *J Virol* 76, 5156–5166.

Pelkmans, L., Kartenbeck, J. & Helenius, A. (2001). Caveolar endocytosis of simian virus 40 reveals a new two-step vesicular-transport pathway to the ER. *Nat Cell Biol* 3, 473–483.

Pileri, P., Uematsu, Y., Campagnoli, S., Galli, G., Falugi, F., Petracca, R., Weiner, A. J., Houghton, M., Rosa, D., Grandi, G. & Abrignani, S. (1998). Binding of hepatitis C virus to CD81. *Science* 282, 938–941.

Ploss, A., Evans, M. J., Gaysinskaya, V. A., Panis, M., You, H., de Jong, Y. P. & Rice, C. M. (2009). Human occludin is a hepatitis C virus entry factor required for infection of mouse cells. *Nature* 457, 882–886.

Sainz, B., Jr, Barretto, N., Martin, D. N., Hiraga, N., Imamura, M., Hussain, S., Marsh, K. A., Yu, X., Chayama, K. & other authors (2012). Identification of the Niemann–Pick C1-like 1 cholesterol absorption receptor as a new hepatitis C virus entry factor. *Nat Med* 18, 281–285.

Scarselli, E., Ansuini, H., Cerino, R., Roccasecca, R. M., Acali, S., Filocamo, G., Traboni, C., Nicosia, A., Cortese, R. & Vitelli, A. (2002). The human scavenger receptor class B type I is a novel candidate receptor for the hepatitis C virus. *Embo J* 21, 5017–5025.

Sieczkarski, S. B. & Whittaker, G. R. (2002a). Dissecting virus entry via endocytosis. *J Gen Virol* 83, 1535–1545.

Sieczkarski, S. B. & Whittaker, G. R. (2002b). Influenza virus can enter and infect cells in the absence of clathrin-mediated endocytosis. *J Virol* 76, 10455–10464.

Sumpter, R., Jr, Loo, Y.-M., Foy, E., Li, K., Yoneyama, M., Fujita, T., Lemon, S. M. & Gale, M., Jr (2005). Regulating intracellular antiviral defense and permissiveness to hepatitis C virus RNA replication through a cellular RNA helicase, RIG-I. *J Virol* 79, 2689–2699.

Suzuki, T., Ishii, K., Aizaki, H. & Wakita, T. (2007). Hepatitis C viral life cycle. *Adv Drug Deliv Rev* 59, 1200–1212.

Suzuki, R., Saito, K., Kato, T., Shirakura, M., Akazawa, D., Ishii, K., Aizaki, H., Kanegae, Y., Matsuura, Y. & other authors (2012). Trans-complemented hepatitis C virus particles as a versatile tool for study of virus assembly and infection. *Virology* 432, 29–38.

Suzuki, R., Matsuda, M., Watashi, K., Aizaki, H., Matsuura, Y., Wakita, T. & Suzuki, T. (2013). Signal peptidase complex subunit 1 participates in the assembly of hepatitis C virus through an interaction with E2 and NS2. *PLoS Pathog* 9, e1003589.

Trotard, M., Lepère-Douard, C., Régeard, M., Piquet-Pellorce, C., Lavillette, D., Cosset, F. L., Gripon, P. & Le Seyec, J. (2009). Kinases required in hepatitis C virus entry and replication highlighted by small interference RNA screening. *FASEB J* 23, 3780–3789.

van der Schaar, H. M., Rust, M. J., Chen, C., van der Ende-Metselaar, H., Wilschut, J., Zhuang, X. & Smit, J. M. (2008). Dissecting the cell entry pathway of dengue virus by single-particle tracking in living cells. *PLoS Pathog* 4, e1000244.

Vieyres, G., Thomas, X., Descamps, V., Duverlie, G., Patel, A. H. & Dubuisson, J. (2010). Characterization of the envelope glycoproteins associated with infectious hepatitis C virus. *J Virol* 84, 10159–10168.

Zhong, J., Gastaminza, P., Cheng, G., Kapadia, S., Kato, T., Burton, D. R., Wieland, S. F., Uprichard, S. L., Wakita, T. & Chisari, F. V. (2005). Robust hepatitis C virus infection *in vitro*. *Proc Natl Acad Sci U S A* 102, 9294–9299.
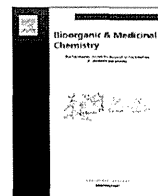
Synthesis of 3′,4′-difluoro-3′-deoxyribonucleosides and its evaluation of the biological activities: Discovery of a novel type of anti-HCV agent 3′,4′-difluorocordycepin

CrossMark

Hisashi Shimada [a], Kazuhiro Haraguchi [b,*], Kumi Hotta [a], Tomoko Miyaike [a], Yasuyuki Kitagawa [c], Hiromichi Tanaka [a], Ryutaro Kaneda [d], Hiroshi Abe [d], Satoshi Shuto [d], Kyoko Mori [e], Youki Ueda [e], Nobuyuki Kato [e], Robert Snoeck [f], Graciela Andrei [f], Jan Balzarini [f]

[a] School of Pharmacy, Showa University, 1-5-8 Hatanodai, Shinagawa-ku, Tokyo 142-8555, Japan
[b] Nihon Pharmaceutical University, 10281 Komuro, Inamachi, Kita-adachi-gun, Saitama 362-0806, Japan
[c] Yokohama College of Pharmacy, 601 Matano-cho, Totsuka-ku, Yokohama-shi, Kanagawa 245-0066, Japan
[d] Faculty of Pharmaceutical Sciences, Hokkaido University, Kita-12, Nishi-6, Kita-ku, Sapporo 060-0812, Japan
[e] Department of Tumor Virology, Okayama University Graduate School of Medicine, Dentistry, and Pharmaceutical Sciences, 2-5-1 Shikata-cho, Okayama 700-8558, Japan
[f] Rega Institute for Medical Research, Katholieke Universiteit Leuven, Minderbroedersstraat 10, B-3000 Leuven, Belgium

ARTICLE INFO

ABSTRACT

Upon reacting 3′,4′-unsaturated cytosine (8 and 9) and adenine nucleosides (13 and 14) with XeF_2/ $BF_3 \cdot OEt_2$, the respective novel 3′,4′-difluoro-3′-deoxyribofuranosyl nucleosides (10–12 and 15–18) could be obtained. Formation of anti-adducts (11, 16 and 18) revealed that the fluorination involved oxonium ions as incipient intermediates. TBDMS-protected 3′,4′-unsaturated adenosine provided the β-face adducts as sole stereoisomers whereas α-face-selectivity was observed with the TBDPS-protected adenosine 14. The evaluation of the novel 3′-deoxy-3′,4′-difluororibofuranosylcytosine-(19–21) and adenine nucleosides (22–25) against antitumor and antiviral activities revealed that 3′,4′-difluorocordycepin (24) was found to possess anti-HCV activity. The SI of 24 was comparable to that of the anti-HCV drug ribavirin. However, sofosbuvir, FDA-approved novel anti-HCV drug, showed better SI value. Our finding revealed that the introduction of the fluoro-substituent into the 4′-position of cordycepin derivatives decreased the cytotoxicity to the host cell with retention of the antiviral activity.

© 2014 Elsevier Ltd. All rights reserved.

1. Introduction

Nucleoside analogues are recognized as an important class of biologically active compounds, especially as antiviral and antitumor agents.[1–4] Among their sugar-modified analogues, fluorinated sugar nucleosides have attracted much attention due to their remarkable antiviral and antitumor activities.[5a] In Figure 1, a selection of antibacterial, antiviral and antitumor derivatives is depicted. Nucleocidin (1) is an antitrypanosomal nucleoside antibiotic and its core structure is 4′-fluoroadenosine. FLT (2) is a synthetic 3′-monofluorinated 3′-deoxythymidine and exhibits anti-HIV activity. 2′-β-Fluorinated thymidine nucleoside, FMAU (3a), has been known to possess antiherpes activity. Quite recently, FDA has approved sofosbuvir (3b), 2′-deoxy-2′-α-fluoro-2′-β-C-methylurodine, for the treatment of chronic hepatitis C.[5b]

Other than monofluoro-sugar derivatives, nucleosides substituted with two fluoro groups in the sugar moiety have been synthesized and evaluated for biological activities. One type of these is the geminally-difluorinated nucleosides, which are depicted in Figure 2. 2′,2′-Geminally-difluorinated 2′-deoxycytidine (gemicitabine, 4) has been well known for treatment of pancreatic cancer.[5a] Its regioisomer, 3′,3′-geminally-difluorinated 3′-deoxycytidine (5a) and thymidine derivative (5b) have also been synthesized.[5a] Another type of difluoro nucleosides are the vicinally-difluorinated derivatives. Four possible isomers (I–IV) have been reported[6] and among them, 2′,3′-dideoxy-2′,3′-difluoro-β-D-arabinofuranosyl cytosine (6) has been reported to show anti-HIV activity (Fig. 3).[7]

In this context, we have been interested in the synthesis and biological evaluation of novel 3′,4′-difluorinated nucleosides V because the respective adenine nucleosides VI are 3′,4′-difluorinated analogues of the nucleoside antibiotic cordycepin[8] (Fig. 4).

A synthetic plan for the target molecules is illustrated in Scheme 1. In the course of our ongoing research on the synthetic chemistry of unsaturated sugar nucleosides,[9] we have already

---
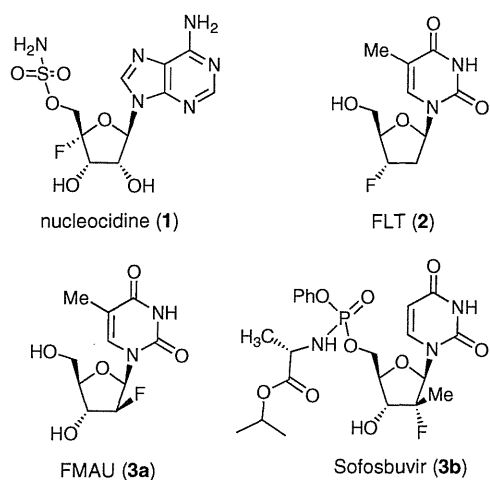
Figure 1. Structure of biologically-active monofluoro compounds 1–3.

gemicitabine (4)

5a: B = cytosin-1-yl,
X = OH
5b: B = thymin-1-yl,
X = H
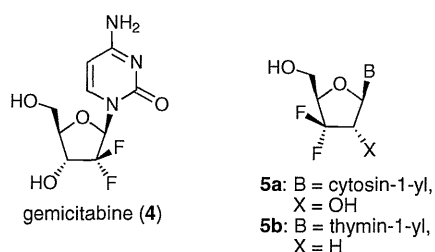
Figure 2. Structure of geminally-difluorinated compounds 4–5.

β-D-ribo (I)

β-D-ara (II)

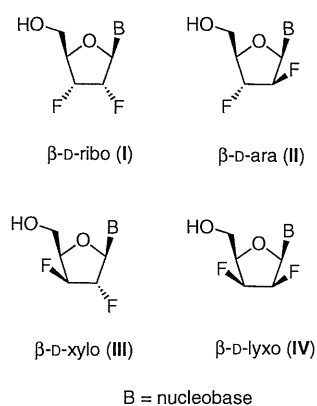β-D-xylo (III)

β-D-lyxo (IV)

B = nucleobase

6

Figure 3. Structure of 2′,3′-vicinal-difluoronucleosides I–IV and anti-HIV agent 6.

reported on the allylic rearrangement of 3′,4′-unsaturated nucleosides leading to 4′-substituted 2′,3′-didehydro-2′,3′-dideoxynucleosides.[10] Aiming at expanding the synthetic utility of 3′,4′-unsaturated nucleosides (VII), we have intended to utilize VII as a substrate for the synthesis of the target molecules. It has been demonstrated that xenon difluoride (XeF$_2$) is a reagent for the

fluorination of unsaturated organic molecules under mild reaction conditions.[11] In the case of alkenes as substrates, 1,2-difluoroalkanes could be obtained.[12] This synthetic method has also been applied to acetylglycal leading to 1,2-difluoro-1,2-dideoxyhexoses.[13,14] We thus envisioned that xenon difluoride-mediated difluorination of 3′,4′-unsaturated nucleosides (VII) would give rise to unprecedented vicinal difluoronucleosides, 3′-deoxy-3′,4′-difluoro-ribonucleoside (VIII). In this paper, we will describe these results and the biological activities of VIII.

2. Results and discussion

2.1. Chemistry

Initially, the di-fluorination of 3′,4′-unsaturated cytosine nucleosides was examined. The substrates 8 and 9 were prepared from 7[10] through de-acetylation and silylation of the resulting diols (Scheme 2). When a benzene solution of BF$_3$·OEt$_2$ (3.0 equiv) was added to an Et$_2$O solution of 8 and XeF$_2$ (1.5 equiv) at 0 °C under Ar atmosphere, the desired vicinal difluorination proceeded and a mixture of the respective 3′-deoxy-3′,4′-difluorocytidine derivatives IX (Pg = TBDMS) was obtained (Scheme 3). To separate these stereoisomers, the silyl-protecting groups were converted into acetyl groups in a one pot manner, and the β-syn-adduct 10 (α-L-arabinofuranosyl isomer) and β-anti-adduct 11 (β-D-xylofuranosyl isomer) could be obtained in 25% and 27% yields, respectively (Table 1, entry 1). The depicted structures were assigned on the basis of NOE experiments; for 10, H-1′/H-3′ (2.1%) and H-3′/H-5′b (1.1%); for 11 H-1′/H-3′ (0.7%) and H-5′a/H-6 (0.6%). In the ^{1}H NMR spectra of 10 and 11, the most significant difference was the coupling pattern of the C1′ proton. Thus, 10 showed vicinal and five-bond long-range coupling ($J_{1′,2′} = J_{1′,4′F} = 6.4$ Hz) whereas 9 showed only a small vicinal coupling ($J_{1′,2′} = 2.4$ Hz). It has been reported that five-bond H–F coupling ($J_{F1,H4} = 6–7$ Hz) occurs in pentofuranosyl fluorides when the C1-F and C4-H functions are trans disposed, whereas the corresponding cis isomers show much smaller values (1–2 Hz).[15,16] This report supported the depicted structures of 10 and 11. Another characteristic difference was the observed four-bond long-range H–F coupling between C5′-H and C3′-F ($J_{F3′,H5′a} = 2.0$ Hz and $J_{F3′,H5′b} = 2.8$ Hz) in 11 (H-5′a and H-5′b coupled as ddd, respectively); this was observed when C5′ and C3-F are in a cis relationship. On the other hand, no such long-range coupling was observed in 10 (H-5′a and H-5′b appeared as dd) in which C5′ and C3′-F are trans disposed.

The stereochemical outcome of the di-fluorination could be rationalized by shielding the α-face of the 3′,4′-double bond with the sterically encumbered 2′-O-TBDMS group leading to the formation of the incipient β-coordinated transition state X and subsequently-formed oxonium ion XI (Fig. 5).

When TBDPS-protected 9 was subjected to the fluorination under the same reaction conditions as for 8, α-syn adduct 12 (β-D-ribofuranosyl isomer) was obtained in 5% isolated yield along with 10 (52%) and 11 (34%) after removal of the TBDPS groups of IX (Pg = TBDPS) and acetylation of the resulting diols (Scheme 3 and entry 2 in Table 1). In the ^{1}H NMR spectrum of 12, the anomeric proton appeared as a doublet and the C5′-proton was observed as a double doublet. Finally, the depicted structure was supported by NOE experiments; H-6/ H-3′ (0.7%), H-6/H-5′b (1.0%), H-2′/H-3′ (5.1%) and H-5′a/ H-3′ (0.5%). The formation of the α-adduct could be explained by the out-side orientation of the 2′-O-TBDPS group to the double bond caused by a buttressing effect of the 5′-O-TBDPS group and the 2′-O-TBDPS group.

Next, the difluorination of the TBDMS-protected adenine nucleoside 13[17] was examined (Scheme 4). Under the above-mentioned reaction conditions, 13 gave a mixture of two stereoisomers XII (Pg = TBDMS). The mixture was subjected to N^6-pivaloylation,
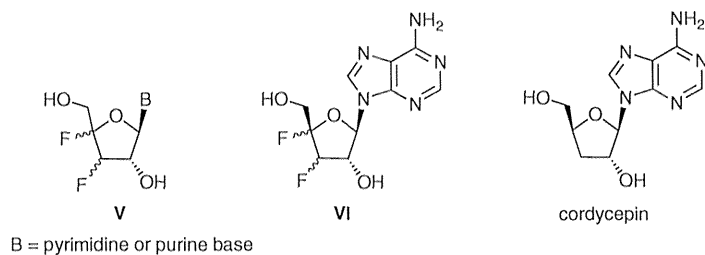
Figure 4. Structure of 3',4'-difluoronucleoside (**V** and **VI**) and cordycepin.
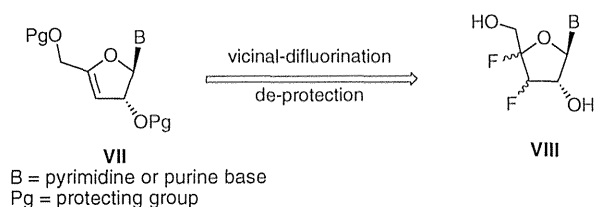
Scheme 1. Synthesis of 3',4'-difluoronucleosides (**VIII**) from 3',4'-unsaturated nucleosides (**VII**).

**Table 1**
XeF$_2$-mediated difluorination of 3',4'-unsaturated cytidine and adenosine derivatives **8, 9, 13** and **14**

| Entry	Substrate	Products (isolated yields, %)				β/α
		β-syn	β-anti	α-syn	α-anti	
1	8	10 (25)	11 (27)	–	–	1/0
2	9	10 (52)	11 (34)	12 (5)	–	1/0.06
3	13	15 (45)	16 (22)	–	–	1/0
4	14	15 (18)	16 (2)	17 (36)	18 (5)	1/2.1
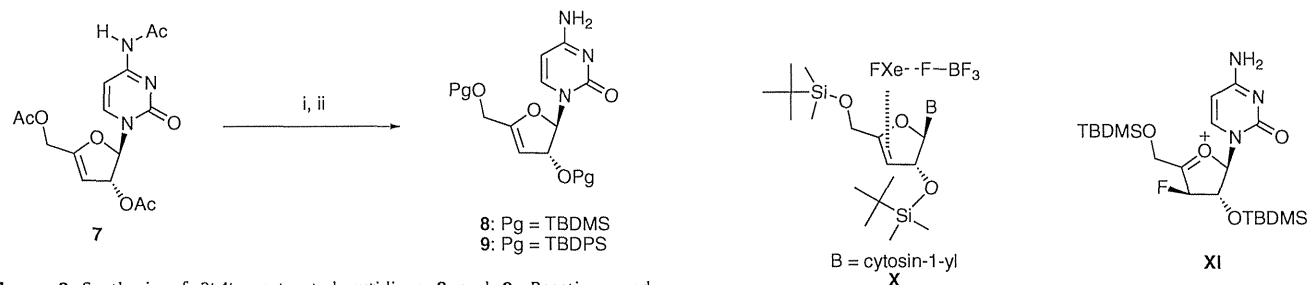
Scheme 2. Synthesis of 3',4'-unsaturated cytidines **8** and **9**. Reactions and conditions: (i) NH$_3$/MeOH; (ii) TBDMSCl or TBDPSCl /imidazole/DMF; **8** (65%), **9** (71%).


Figure 5. Plausible transition state **X** and oxonium ion **XI** in the fluorination of **8**.
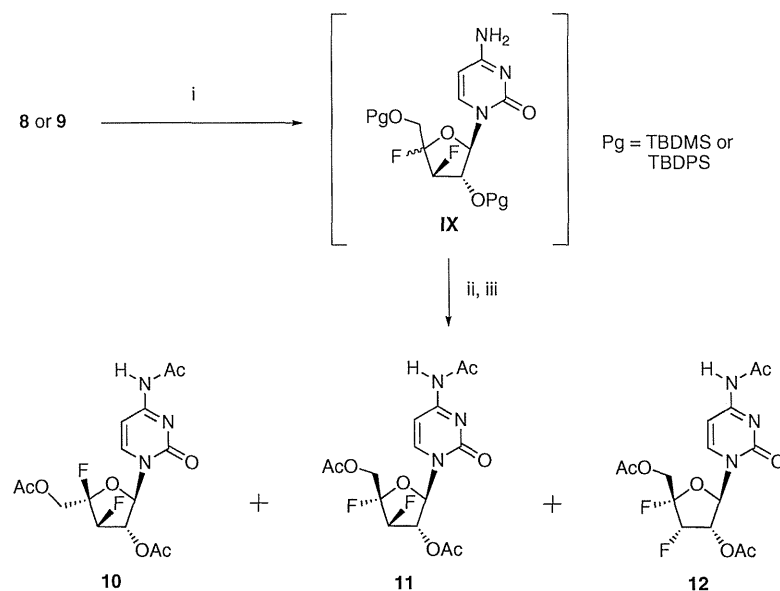

Scheme 3. Reaction of 3',4'-unsaturated cytidines **8** and **9** with XeF$_2$/BF$_3$·OEt$_2$: Formation of **10, 11** and **12**. Reactions and conditions: (i) XeF$_2$, BF$_3$·OEt$_2$, ether–benzene; (ii) Bu$_4$NF/THF; (iii) Ac$_2$O.
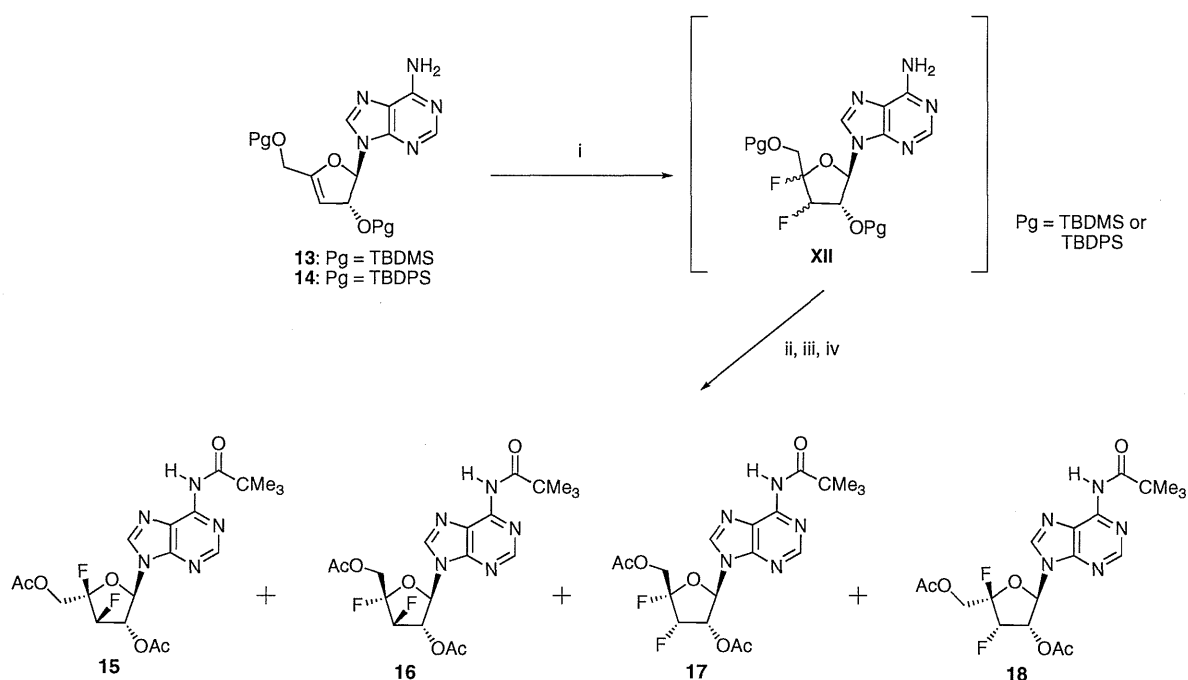
Scheme 4. XeF$_2$-mediated difluorination of **13** and **14**: Formation of **15–18**. Reactions and conditions: (i) XeF$_2$, BF$_3$·OEt$_2$, ether–benzene; (ii) Me$_3$CCOCl/*i*-Pr$_2$NEt/CH$_2$Cl$_2$; (iii) Bu$_4$NF/THF; (iv) Ac$_2$O.
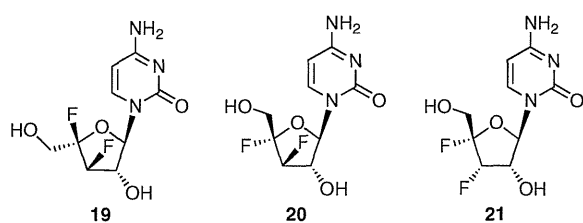
Figure 6. Structure of compounds **19–21**.
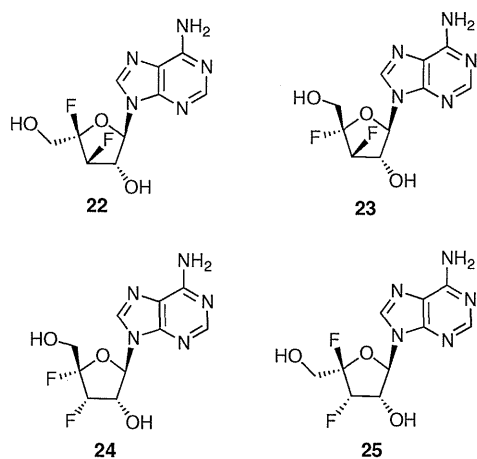
Figure 7. Structure of compounds **22–25**.

Figure 8. Theoretical calculation of potential energies of **23** and **24** during one full pseudorotation cycle.

(2%). Although it is not clear why the fluorination of **14** proceeded with α-face-selectively, it would be reasonable that the sterically-encumbered adenine base plays an important role in this process.

The fluorinated cytosine **10–12** and adenine nucleosides **15–18** were de-protected to furnish the target molecules **19–21** (Fig. 6) and **22–25** (Fig. 7).

2.2. Theoretical calculations

In order to examine the influence of the introduced two fluorine substituents on the puckering of the furanose moiety, molecular orbital calculations were performed to determine the relative energies of the pseudo rotation phase angles of the β-ᴅ-xylofurano-

de-silylation and acetylation of the resulting diols to give the β-*syn*-**15** (45%) and the β-*anti*-adduct **16** (22%) (entry 3, Table 1). This stereochemical outcome is consistent with that of the cytosine nucleoside **8**. Interestingly, as shown by entry 4 in Table 1, the fluorination of the TBDPS-protected **14**[17] was found to proceed with α-face selectively to provide the α-*syn*-adduct **17** as the major product (36%) along with the α-*anti*-adduct **18** (5%), **15** (18%) and **16**

6178

H. Shimada et al./Bioorg. Med. Chem. 22 (2014) 6174–6182

23 (P = 150°)
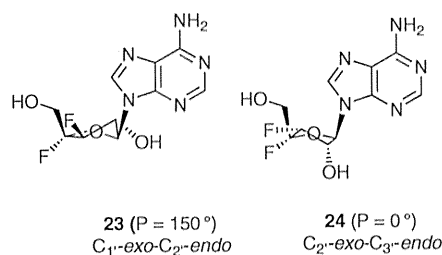C$_1$'-*exo*-C$_2$'-*endo*

24 (P = 0°)
C$_2$'-*exo*-C$_3$'-*endo*

Figure 9. Calculated preferential conformation of **23** and **24**.

syl isomer **23** and the β-D-ribofuranosyl isomer **24** (Fig. 8). The energies of the respective puckerings were calculated at the HF/3-21G* level using the Gaussian 09 program 20. As a reference molecule, the result of cordycepin is included. As can be seen in Figure 8, cordycepin adopted the C$_2$'-*exo*-C$_3$'-*endo* (P = 0°) puckering as a preferential conformation,[18] which is consistent with the X-ray crystallographic analysis.[19] Compound **23** was found to adopt C$_1$'-*exo*-C$_2$'-*endo* (P = 150°) puckering as depicted in Figure 9. On the other hand, **24** had C$_2$'-*exo*-C$_3$'-*endo* (P = 0°) puckering as for cordycepin. Two major known stereoelectronic effects for the specific arrangement of substituents on a furanose-ring are the gauche effect (GE) and antiperiplanar effect (AP).[20] The preferred gauche conformation observed for systems X–C–C–Y, where X and Y are strongly electronegative groups, is able to explain the GE whereas the AP purports that the most electronegative substituent prefers to be anti to the least electronegative one. As can be seen in Figure 9, in both cases of **23** and **24**, the relative arrangement of the fluoro-substituents in F–C3'–C4'–F is *gauche* and that of 4'-fluoro- and C2' in C–C3'–C4'–F is nearly *anti*-conformation. These calculated results would imply that the preferential sugar puckering in **23** and **24** is governed by synergic influences of GE and AP.

2.3. Biological evaluation

It has been reported that cordycepin exhibits antitumor activity.[8] Therefore, the novel 3'-deoxy-3',4'-difluoroadenosine derivatives (**22–25**) were evaluated on the proliferation of murine leukemia cells and human cervix carcinoma. None of these novel molecules showed inhibitory activities against these tumor cell lines. Evaluation against antiviral activities was also carried out and no inhibitory activities against human cytomegalovirus, herpes simplex virus, vesicular stomatitis virus and varicella-zoster-virus. In the above biological evaluation, **22–25** did not show any cytotoxicities against host cells at 100 μM. On the other hand, anti-HCV assay[21,22] of **19–25** revealed that 3'-deoxy-3', 4'-difluoroadenosine **24** (3',4'-difluorocordycepin) exhibited inhibitory activity (EC$_{50}$ of 4.7 μM) (Table 2) whereas the parent molecule cordycepin did not show significant anti-HCV activity. The

Table 2
Anti-HCV activity of **19–25**

Compound	EC$_{50}$[a] (μM)	CC$_{50}$[b] (μM)	SI[c]
19	>100	23	<0.23
20	>100	36	<0.36
21	>50	>50	<1.0
22	>100	>100	>1
23	>200	>200	>1
24	4.7	90	19
25	>200	>200	>1
Ribavirin	5.6	100	18
Sofosbuvir	0.14	>5.0	>36
Cordycepin	70	13	0.19

[a] RL assay.[21]
[b] WST-1 cell proliferation assay.[22]
[c] CC$_{50}$/EC$_{50}$.

activity and toxicity profile (IC$_{50}$ of 90 μM, SI of 19) is comparable to that of anti-HCV drug ribavirin (EC$_{50}$ of 5.6 μM, IC$_{50}$ of 100 μM, SI of 18). However, FDA-approved NS5B inhibitor sofosbuvir showed better profile (EC$_{50}$ of 0.14 μM, IC$_{50}$ of >5.0 μM, SI of >36 μM). As mentioned above, 3',4'-difluorocordycepin **24** did not show significant cytotoxicities to the host cell lines. Therefore, the observed activity would be attributed to the inhibition of NS5B polymerase. It has been reported that 3'-deoxy-3'-fluoroadenosine (3'-fluorocordycepin) exhibits inhibitory activity against HCV (EC$_{50}$ 1.2 μM) but is highly toxic to host cell.[23] It is possible to mention, therefore, that introduction of the fluorine substituent into the 4'-position of 3'-fluorocordycepin gave rise to decrease its cytotoxicity with retention of inhibitory activity against HCV.

3. Conclusions

We have developed a synthetic method for the novel 3'-deoxy-3',4'-difluorocytosine and adenine nucleosides. XeF$_2$-mediated difluorination of 2',5'-bis-*O*-silyl-protected 3',4'-unsaturated cytidines (**8** and **9**) proceeded with β-face selectively to give β-*syn*-(**10**) and β-*anti*-adduct (**11**) as the major isomers. On the other hand, 2',3'-bis-*O*-TBDPS-protected 3',4'-unsaturated adenosine (**14**) provided the α-*syn*-adduct (**17**) as the major product. Removal of the protecting groups of cytidine derivatives **10–12** and adenosine derivatives **15–18** provided the target nucleosides **19–25** in good isolated yields. Theoretical calculation of potential energies of the 3',4'-difluoro derivatives **23** and **24** of cordycepin revealed that the preferential sugar-puckering modes are controlled by synergistic influences of GE and AP.

Evaluation of antiviral activities of the novel 3'-deoxy-3', 4'-difluorocytidine and adenosine derivatives revealed that 3',4'-difluorocordycepin **24** showed anti-HCV activity comparable potency to that of the anti-HCV drug rivabirin. The fact that **24** and inactive cordycepin have similar preferential sugar puckering (C$_2$'-*exo*-C$_3$'-*endo*) suggested that intermolecular interaction of the 3' and 4'-fluoro-substituents with target enzyme may play an important role for anti-HCV activity. Our finding concerning biological evaluation revealed that the introduction of the fluoro-substituent into the 4'-position of cordycepin derivatives decreased the cytotoxicity to the host cell with retention of the antiviral activity. Further studies concerning its action of mechanism of the anti-HCV activity as well as the SAR are underway.

4. Methods

4.1. General methods

Melting points are uncorrected. ^{1}H and ^{13}C NMR spectra were recorded either at 400 MHz or at 500 MHz. Chemical shifts are reported relative to Me$_4$Si. Mass spectra (MS) were taken in FAB mode with *m*-nitrobenzyl alcohol as a matrix. Column chromatography was carried out on silica gel. Thin-layer chromatography (TLC) was performed on silica gel. When necessary, analytical samples were purified by high performance liquid chromatography (HPLC). THF was distilled from benzophenone ketyl.

4.2. 1-[2,5-Bis-*O*-(*tert*-butyldimethylsilyl)-β-D-*glycero*-pent-3-enofuranosyl]cytosine (8)

To a solution of **7** (270.5 mg, 0.77 mmol) in MeOH (15 mL) was added NaOMe (304.1 mg, 5.63 mmol) under Ar atmosphere at 0 °C and the mixture was stirred overnight. The reaction mixture was neutralized with AcOH and chromatographed on a silica gel (25% MeOH in CH$_2$Cl$_2$) to give the respective triol. To a solution of the triol in DMF (3.5 mL) was added imidazole (209.7 mg, 3.08 mmol) and *tert*-butylchlorodimethylsilane (348.1 mg, 2.31 mmol) under Ar atmosphere at 0 °C and the mixture was stirred overnight at

rt. The reaction mixture was partitioned between AcOEt and H_2O and silica gel column chromatography (3% MeOH in CH_2Cl_2) of the organic layer gave **8** (226.3 mg, 65%) as foam: ^1H NMR (CDCl$_3$) δ 0.09, 0.11, 0.12 and 0.14 (12H, each as s, Si-Me), 0.89 and 0.92 (18H, each as s, Si-*tert*-Bu), 4.27 (2H, s, CH$_2$-5′), 4.75–4.77 (1H, m, H-3′), 5.12 (1H, t, $J_{1',2'} = J_{2',3'} = 1.1$ Hz, H-2′), 5.64 (1H, d, $J_{5,6} = 7.4$ Hz, H-5), 6.32 (1H, t, $J_{1',2'} = 1.1$ Hz, H-1′), 7.28 (1H, d, $J_{5,6} = 7.4$ Hz, H-6); ^{13}C NMR (CDCl$_3$) δ -5.4, -5.4, -4.8, -4.5, 18.1, 18.3, 25.8, 58.5, 80.5, 93.8, 94.6, 101.0, 140.2, 155.3, 165.8; FAB-MS (m/z) 454 (M$^+$+H). Anal. Calcd for C$_{21}$H$_{39}$N$_3$O$_4$Si$_2$: C, 55.59; H, 8.66; N, 9.26. Found: C, 55.62; H, 8.45; N, 9.15.

4.3. 1-[2,5-Bis-*O*-(*tert*-butyldiphenylsilyl)-β-D-*glycero*-pent-3-enofuranosyl]cytosine (9)

To a solution of **7** (617.4 mg, 1.76 mmol) in MeOH (15 mL) was added NaOMe (304.1 mg, 5.63 mmol) under Ar atmosphere at 0 °C and the mixture was stirred overnight. The reaction mixture was neutralized with AcOH and chromatographed on a silica gel (25% MeOH in CH_2Cl_2) to give the respective triol. To a solution of the triol in DMF (7 mL) was added imidazole (479.3 mg, 7.04 mmol) and *tert*-butylchlorodiphenylsilane (1.4 mL, 5.28 mmol) under Ar atmosphere at 0 °C and the mixture was stirred overnight at rt. The reaction mixture was partitioned between AcOEt and H_2O and silica gel column chromatography (3% MeOH in CH_2Cl_2) of the organic layer gave **9** (875.0 mg, 71%) as solid: mp 98–101 °C; ^1H NMR (CDCl$_3$) δ 1.02 and 1.06 (18H, each as Si-*tert*-Bu), 4.17 (2H, s, CH$_2$-5′), 4.78–4.81 (2H, m, H-2′ and H-3′), 6.66 (1H, d, $J_{1',2'} = 1.7$ Hz, H-1′), 7.00 (1H, d, $J_{5,6} = 7.4$ Hz, H-5), 7.35–7.38 and 7.62–7.72 (21H, each as m, Ph and H-6); ^{13}C NMR (CDCl$_3$) δ 19.1, 19.2, 26.7, 26.8, 59.1, 81.2, 93.5, 94.8, 100.5, 127.8, 127.8, 127.8, 129.7, 129.8, 129.9, 132.8, 132.9, 133.9, 135.5, 135.5, 135.7, 135.9, 140.2; FAB-MS (m/z) 702 (M$^+$+H). Anal. Calcd for C$_{41}$H$_{47}$N$_3$O$_4$Si$_2$: C, 70.15; H, 6.75; N, 5.99. Found: C, 70.01; H, 6.63; N, 5.87.

4.4. Difluorination of 8

4.4.1. Formation of *N*⁴-Acetyl-1-[2,5-di-*O*-acetyl-3-deoxy-3,4-difluoro-α-L-arabinofuranosyl]cytosine (10) and *N*⁴-Acetyl-1-[2,5-di-*O*-acetyl-3-deoxy-3,4-difluoro-β-D-xylofuranosyl]cytosine (11)

To a solution of **8** (106.4 mg, 0.23 mmol) in Et$_2$O (2.5 mL) was added XeF$_2$ (56.8 mg, 0.35 mmol) and a solution of BF$_3$·OEt$_2$ (87 μL, 0.69 mmol) in benzene (3.5 mL) and the mixture was stirred at 0 °C under Ar atmosphere for 7 h. The reaction mixture was partitioned between CHCl$_3$ and saturated aqueous NaHCO$_3$. Silica gel column chromatography (4–6% MeOH in CH_2Cl_2) of the organic layer gave a mixture of the two stereoisomers of the respective difluorides **IX** (Pg = TBDMS). To a solution of the **IX** (73.5 mg, 0.15 mmol) in THF (3.5 mL) was added Bu$_4$NF (1.0 M THF solution) (0.53 mL 0.53 mmol) and the mixture was stirred at 0 °C under Ar atmosphere for 3.0 h. To the reaction mixture was added Ac$_2$O (57 μL, 0.60 mmol) at 0 °C and the reaction mixture was stirred for 7 h at rt under Ar atmosphere. The reaction mixture was partitioned between CHCl$_3$/saturated NaHCO$_3$ and silica gel column chromatography (hexane/ethyl acetate = 1/1) of the organic layer gave a mixture of **10** and **11**. The mixture was chromatographed by preparative TLC (hexane/ethyl acetate = 1/4) to give **10** (14.9 mg, 25%, foam) and **11** (16.4 mg, 27%, foam).

4.4.1.1. Physical data for 10. ^1H NMR (CDCl$_3$) δ 2.14, 2.16 and 2.26 (9H, each as s, Ac), 4.33 (1H, dd, $J_{4'F,5'a} = 6.0$ and $J_{5'a,5'b} = 12.4$ Hz, H-5′a), 4.44 (1H, dd, $J_{4'F,5'b} = 10.0$ and $J_{5'a,5'b} = 12.4$ Hz, H-5′b), 5.24 (1H, ddd, $J_{2',3'} = 8.0$, $J_{3',4'F} = 17.0$ and $J_{3',3'F} = 51.5$ Hz, H-3′), 5.61–5.69 (1H, m, H-2′), 6.54 (1H, t, $J_{1',2'} = J_{1',4'F} = 6.4$ Hz, H-1′), 8.57 (1H, d, $J_{5,6} = 7.6$ Hz, H-5), 7.89 (1H, d, $J_{5,6} = 7.6$ Hz, H-6), 9.60 (1H, br, NH); NOE (500 MHz, CDCl$_3$): irradiated H-1′/observed H-

3′(2.1%), irradiated H-5′b/observed H-3′ (1.1%); ^{13}C NMR (CDCl$_3$) δ 14.2, 20.4, 20.5, 25.0, 60.4, 68.1, 60.7, 76.2, 76.3, 85.55, 85.64, 88.6, 88.8, 90.3, 90.5, 98.4, 111.9, 112.0, 113.7, 113.9, 143.2, 154.9, 163.3, 169.7, 169.7, 170.8; FAB-MS (m/z) 390 (M$^+$+H). Anal. Calcd for C$_{15}$H$_{17}$F$_2$N$_3$O$_7$ 1/10AcOEt: C, 46.46; H, 4.51; N, 10.55. Found: C, 46.70; H, 4.45; N, 10.79.

4.4.1.2. Physical data for 11. ^1H NMR (CDCl$_3$) 2.16, 2.19 and 2.26 (9H, each as s, Ac), 4.43 (1H, ddd, $J_{3'F,5'a} = 2.0$, $J_{4'F,5'a} = 12.6$. and $J_{5'a,5'b} = 12.4$ Hz, H-5′a), 4.67 (1H, dt, $J_{3'F,5'b} = 2.8$ and $J_{4'F,5'a} = J_{5'a,5'b} = 12.2$ Hz, H-5′b), 5.14 (1H, dd, $J_{2',3'} = 3.2$ and $J_{3',3'F} = 48.0$ Hz, H-3′), 5.27–5.31 (1H, m, H-2′), 6.55 (1H, d, $J_{1',2'} = 2.0$ Hz, H-1′), 7.51 (1H, d, $J_{5,6} = 7.6$ Hz, H-5), 7.66 (1H, d, $J_{5,6} = 7.6$ Hz, H-6), 9.02 (1H, br, NH); NOE (500 MHz, CDCl$_3$): irradiated H-5′a/observed H-6 (2.1%), irradiated H-1′/observed H-3′ (0.7%); ^{13}C NMR (CDCl$_3$) δ 14.2, 20.47, 20.53, 25.0, 29.7, 60.5, 60.7, 78.09, 78.14, 91.2, 92.7, 93.1, 94.2, 94.6, 98.1, 115.7, 115.9, 117.5, 117.7, 143.2, 154.4, 163.4, 169.3, 169.7, 171.1; FAB-MS (m/z) 390 (M$^+$+H). Anal Calcd for C$_{15}$H$_{17}$N$_3$O$_7$ 1/4AcOEt: C, 46.72; H, 4.66; N, 10.21. Found: C, 47.08; H, 4.52; N, 10.46.

4.5. Difluorination of 9

4.5.1. Formation of 10, 11 and *N*⁴-acetyl-1-[2,5-di-*O*-acetyl-3-deoxy-3,4-difluoro-β-D-ribofuranosyl]cytosine (12)

To a solution of **9** (151.2 mg, 0.22 mmol) in Et$_2$O (3.5 mL) was added XeF$_2$ (53.6 mg, 0.33 mmol) and a solution of BF$_3$·OEt$_2$ (84 μL, 0.66 mmol) in benzene (4.5 mL) and the mixture was stirred at 0 °C under Ar atmosphere for 7 h. The reaction mixture was partitioned between CHCl$_3$ and saturated aqueous NaHCO$_3$. Silica gel column chromatography (2% MeOH in CH_2Cl_2) of the organic layer gave a mixture of the three stereoisomers of the respective difluorides **IX** (Pg = TBDPS). To a solution of the **IX** (138.5 mg, 0.19 mmol) in THF (5 mL) was added Bu$_4$NF (1.0 M THF solution) (0.67 mL 0.67 mmol) and the mixture was stirred at 0 °C under Ar atmosphere for 3.0 h. To the reaction mixture was added Ac$_2$O (72 μL, 0.76 mmol) at 0 °C and the reaction mixture was stirred for 7 h at rt under Ar atmosphere. The reaction mixture was partitioned between CHCl$_3$/saturated NaHCO$_3$ and silica gel column chromatography (2% MeOH in CH_2Cl_2) of the organic layer gave a mixture of **10**, **11** and **12**. The mixture was chromatographed by preparative TLC (hexane/ethyl acetate = 1/4) to give **10** (44.5 mg, 52%, foam), **11** (29.1 mg, 34%, foam) and **12** (4.3 mg, 5%, foam).

4.5.1.1. Physical data for 12. ^1H NMR (CDCl$_3$) δ 2.13, 2.20 and 2.24 (9H, each as s, Ac), 4.37 (1H, dd, $J_{4'F,5'a} = 8.4$ and $J_{5'a,5'b} = 12.3$ Hz, H-5′a), 4.57 (1H, dd, $J_{4'F,5'b} = 10.9$ and $J_{5'a,5'b} = 12.3$ Hz, H-5′b), 5.56 (1H, d, $J_{1',2'} = 1.4$ Hz, H-1′), 5.69 (1H, dd, $J_{1',2'} = 1.4$ and $J_{2',3'} = 6.8$ Hz, H-2′), 5.82 (1H, ddd, $J_{2',3'} = 7.4$, $J_{3',4'F} = 17.7$ and $J_{3',3'F} = 49.4$ Hz, H-3′), 7.44 (1H, d, $J_{5,6} = 7.4$ Hz, H-5), 7.51 (1H, d, $J_{5,6} = 7.4$ Hz, H-6), 8.52 (1H, br, NH); NOE (500 MHz, CDCl$_3$): NOE (500 MHz, CDCl$_3$): irradiated H-5′a/observed H-3′ (0.5%), irradiated H-6/observed H-3′ (0.7%), irradiated H-6/observed H-5′b (1.0%), irradiated H-2′/observed H-3′ (5.1%); ^{13}C NMR (CDCl$_3$) δ 14.1, 20.6, 23.0, 23.7, 29.7, 61.1, 61.4, 69.2, 70.5, 70.6, 97.0, 97.6, 128.5, 128.6, 128.8, 130.9, 131.0, 132.07, 132.14, 132.5, 148.1, 154.0, 167.8, 167.0, 170.3; FAB-MS (m/z): 390 (M$^+$+H). HRMS (ESI) (m/z): calcd for C$_{15}$H$_{18}$N$_3$O$_7$F$_2$: 390.11073, found: 390.11057 (M$^+$+H).

4.6. Difluorination of 13

4.6.1. 9-[2,5-Di-*O*-acetyl-3-deoxy-3,4-difluoro-α-L-arabinofuranosyl]-*N*⁶-pivaloyladenine (15), 9-[2,5-di-*O*-acetyl-3-deoxy-3,4-difluoro-β-D-xylofuranosyl]-*N*⁶-pivaloyladenine (16)

To a solution of **13** (63.1 mg, 0.18 mmol) in Et$_2$O (2.5 mL) was added XeF$_2$ (32.5 mg, 0.20 mmol) and a solution of BF$_3$·OEt$_2$

(49.0 μL, 0.39 mmol) in benzene (2.5 mL) and the mixture was stirred at 0 °C under Ar atmosphere for 7 h. The reaction mixture was partitioned between $CHCl_3$ and saturated aqueous $NaHCO_3$. Silica gel column chromatography (hexane/AcOEt = 1/1) of the organic layer gave a mixture of the two stereoisomers of the respective difluorinated products **XII** (Pg = TBDMS). To a solution of the **XII** (66.1 mg, 0.13 mmol) in CH_2Cl_2 (3.5 mL) was added i-Pr$_2$NEt (35 mL, 0.2 mmol) and Me$_3$CCOCl (20 μL, 0.16 mmol) under Ar atmosphere at 0 °C and the mixture was stirred for 5 h at rt. The reaction mixture was partitioned between $CHCl_3$ and saturated aqueous $NaHCO_3$. Silica gel column chromatography (hexane/AcOEt = 4/1) of the organic layer gave a mixture of the respective N^6-pivaloylated products. To a solution of the N^6-pivaloyladenine nucleosides (77.0 mg, 0.13 mmol) in THF (3.5 mL) was added Bu$_4$NF (1.0 M THF solution) (0.33 mL 0.33 mmol) and the mixture was stirred at 0 °C under Ar atmosphere for 2 h. To the mixture was added Ac$_2$O (49.0 μL, 0.52 mmol) and the reaction mixture was stirred for 12 h at 0 °C under Ar atmosphere. The reaction mixture was partitioned between $CHCl_3$/saturated $NaHCO_3$ and silica gel column chromatography (2% MeOH in CH_2Cl_2) of the organic layer gave a mixture of **15** and **16**. The compounds **15** and **16** were separated by preparative TLC (hexane/ethyl acetate = 1/4) to give **15** (44.2 mg, 45%, foam), **16** (16.6 mg, 22%, foam).

4.6.1.1. Physical data for 15.

^{1}H NMR (CDCl$_3$) δ 1.40 (9H, s, CO-tert-Bu). 2.13 and 2.16 (6H, each as s, Ac), 4.35 (1H, dd, $J_{4'F,5'a}$ = 6.6 and $J_{5'a,5'b}$ = 12.2 Hz, H-5′a), 4.53 (1H, dd, $J_{4'F,5'b}$ = 9.8 and $J_{5'a,5'b}$ = 12.2 Hz, H-5′b), 5.32 (1H, ddd, $J_{2',3'}$ = 7.2, $J_{3',4'F}$ = 17.2 and $J_{3',3'F}$ = 51.2 Hz, H-3′), 6.11 (1H, ddd, $J_{1',2'}$ = 5.6, $J_{2',3'}$ = 7.2 and $J_{2',3'F}$ = 16.0 Hz, H-2′), 6.46 (1H, t, $J_{1',2'}$ = $J_{1',4'F}$ = 5.4 Hz, H-1′), 8.34 (1H, s, H-8), 8.61 (1H, br, NH) and 8.74 (1H, s, H-2); NOE (500 MHz, CDCl$_3$): irradiated H-1′/observed H-3′ (2.6%), irradiated H-3′/observed H-5′a (1.2%) and irradiated H-5′b/observed H-3′ (1.2%); ^{13}C NMR (CDCl$_3$) δ 20.3, 20.5, 27.4, 40.6, 60.5, 60.8, 83.6, 83.7, 89.6, 89.8, 91.3, 91.4, 112.0, 112.2, 113.9, 114.0, 122.3, 139.96, 140.01, 149.8, 151.7, 153.2, 169.4, 169.7, 175.6; FAB-MS (m/z) 456 (M$^+$+H). Anal. Calcd for C$_{19}$H$_{43}$F$_2$N$_5$O$_6$: C, 50.11; H, 5.09; N, 15.38. Found: C, 49.92; H, 5.06; N, 15.18.

4.6.1.2. Physical data for 16.

^{1}H NMR (CDCl$_3$) δ 1.41 (9H, s, CO-tert-Bu). 2.16 and 2.21 (6H, each as s, Ac), 4.44 (1H, ddd, $J_{3'F,5'a}$ = 2.4, $J_{4'F,5'a}$ = 21.6 and $J_{5'a,5'b}$ = 12.4 Hz, H-5′a), 4.61 (1H, dt, $J_{3'F,5'b}$ = $J_{4'F,5'b}$ = 12.2 and $J_{5'a,5'b}$ = 12.2 Hz, H-5′b), 5.29 (1H, dd, $J_{2',3'}$ = 3.6 and $J_{3',3'F}$ = 48.4 Hz, H-3′), 5.64–5.69 (1H, m, H-2′), 6.66 (1H, d, $J_{1',2'}$ = 2.4 Hz, H-1′), 8.11 (1H, s, H-8), 8.52 (1H, br, NH) 8.77 (1H, s, H-2); NOE (500 MHz, CDCl$_3$): irradiated H-3′/observed H-1′ (0.8%) and irradiated H-5′a/observed H-8 (0.7%); ^{13}C NMR (CDCl$_3$) δ 20.4, 20.5, 27.4, 40.5, 60.6, 60.8, 78.0, 78.3, 88.3, 93.1, 93.4, 94.6, 94.9, 115.5, 115.76, 115.77, 117.4, 117.6, 122.6, 140.07, 140.11, 142.2, 149.9, 151.6, 153.0, 153.2, 153.3, 169.4, 169.6, 175.7; FAB-MS (m/z) 456 (M$^+$+H); Anal Calcd for C$_{19}$H$_{23}$F$_2$N$_5$O$_6$ 1/10AcOEt: C, 50.19; H, 5.13; N, 15.08. Found: C, 50.30; H, 5.12; N, 14.86.

4.7. Difluorination of 14

4.7.1. Formation of 15, 16, 9-[2,5-Di-O-acetyl-3-deoxy-3,4-difluoro-β-D-ribofuranosyl]-N^6-pivaloyladenine (17) and 9-[2,5-Di-O-acetyl-3-deoxy-3,4-difluoro-α-L-lyxofuranosyl]-N^6-pivaloyladenine (18)

To a solution of **14** (318.2 mg, 0.44 mmol) in Et$_2$O (5.0 mL) was added XeF$_2$ (107.1 mg, 0.66 mmol) and BF$_3$·OEt$_2$ (0.17 mL, 1.32 mmol) in benzene (6.0 mL) and the mixture was stirred at 0 °C under Ar atmosphere for 4 h. The reaction mixture was partitioned between $CHCl_3$ and saturated aqueous $NaHCO_3$. Silica gel

column chromatography (hexane/AcOEt = 1/1) of the organic layer gave a mixture of the three stereoisomers of the respective difluorinated adenine nucleosides **XII** (Pg = TBDPS). To a solution of the **XII** (298.5 mg, 0.39 mmol) in CH_2Cl_2 (7.0 mL) was added i-Pr$_2$NEt (0.1 mL, 0.59 mmol) and pivaloyl chloride (58.0 μL, 0.47 mmol) and the mixture was stirred at 0 °C under Ar atmosphere for 6 h. The reaction mixture was partitioned between $CHCl_3$ and saturated $NaHCO_3$ and silica gel column chromatography (hexane/ethyl acetate = 2/1) of the organic layer gave N^6-pivaloylated products (303.6 mg, 92%). To a solution of N^6-pivaloylated products (303.6 mg, 0.36 mmol) in THF (6.0 mL) was added Bu$_4$NF (1.0 M THF solution) (0.9 mL 0.9 mmol) and the mixture was stirred at 0 °C under Ar atmosphere for 1.5 h. To the mixture was added Ac$_2$O (0.14 mL, 1.44 mmol) and the reaction mixture was stirred for 7 h at 0 °C under Ar atmosphere. The reaction mixture was partitioned between $CHCl_3$/saturated $NaHCO_3$ and silica gel column chromatography (hexane/ethyl acetate = 1/2) of the organic layer gave a mixture of **15–18**. Preparative TLC (hexane/ethyl acetate = 1/4) of the mixture gave **15** (29.5 mg, 18%, foam), **16** (3.3 mg, 2%, foam), **17** (59.0 mg, 36%, foam) and **18** (8.2 mg, 5%, foam).

4.7.1.1. Physical data for 17.

^{1}H NMR (CDCl$_3$) δ 1.40 (9H, s, CO-tert-Bu). 2.01 and 2.21 (6H, each as s, Ac), 4.37 (1H, dd, $J_{4'F,5'a}$ = 7.0 and $J_{5'a,5'b}$ = 12.2 Hz, H-5′a), 4.52 (1H, dd, $J_{4'F,5'b}$ = 10.4 and $J_{5'a,5'b}$ = 12.2 Hz, H-5′b), 5.95–5.97 (1H, m, H-2′), 6.13 (1H, ddd, $J_{2',3'}$ = 6.8, $J_{3',4'F}$ = 16.6 and $J_{3',3'F}$ = 48.6 Hz, H-3′), 6.29 (1H, d, $J_{1',2}$ = 2.4 Hz, H-1′), 8.06 (1H, br, NH), 8.55 and 8.74 (2H, each as s, H-2 and H-8); NOE (500 MHz, CDCl$_3$): irradiated H-2′/observed H-3′ (5.3%), irradiated H-3′/observed H-5′a (0.8%), irradiated H-3′/observed H-5′b (1.1%), irradiated H-8/observed H-3′ (0.5%), irradiated H-8/observed H-5′b (1.2%); ^{13}C NMR (CDCl$_3$) δ 20.5, 27.4, 40.6, 60.9, 61.2, 70.6, 70.7, 89.1, 123.6, 142.2, 150.1, 150.9, 153.0, 169.7, 769.8, 175.7; FAB-MS (m/z) 456 (M$^+$+H); Anal. Calcd for C$_{19}$-H$_{23}$F$_2$N$_5$O$_6$ 1/4C$_6$H$_{14}$ 1/2AcOEt: C, 51.87; H, 5.90; N, 13.44. Found: C, 52.27; H, 5.50; N, 13.40.

4.7.1.2. Physical data for 18.

^{1}H NMR (CDCl$_3$) δ 1.41 (9H, s, CO-tert-Bu). 2.14 and 2.15 (6H, each as s, Ac), 4.39 (1H, ddd, $J_{3'F,5'a}$ = 2.8, $J_{4'F,5'a}$ = 12.8 and $J_{5'a,5'b}$ = 12.6 Hz, H-5′a), 4.57 (1H, ddd, $J_{3'F,5'b}$ = 3.2, $J_{4'F,5'b}$ = 12.6 and $J_{5'a,5'b}$ = 12.6 Hz, H-5′b), 5.36–5.50 (1H, m, H-3′), 5.97 (1H, ddd, $J_{2',3'}$ = 4.0, $J_{2',4'F}$ = 3.2 and $J_{2',3'F}$ = 23.2 Hz, H-2′), 6.72 (1H, dd, $J_{1',2'}$ = 5.6 and $J_{1',4'F}$ = 6.8 Hz, H-1′), 8.20 (1H, s, H-8), 8.46 (1H, br, NH) and 8.77 (1H, s, H-2); NOE (500 MHz, CDCl$_3$): irradiated H-2′/observed H-3′ (7.2%); ^{13}C NMR (CDCl$_3$) δ 20.3, 20.6, 28.5, 40.6, 60.5, 60.7, 73.9, 74.0, 85.9, 88.0, 88.4, 89.6, 89.9, 115.9, 116.0, 117,7, 117,9, 123.0, 128.9, 131.0, 128.9, 131.0, 132.3, 140,4, 149.9, 152.1, 153.3, 169.6, 169.7, 175.8; FAB-MS (m/z) 456 (M$^+$+H); HRMS (ESI) (m/z): calcd for C$_{19}$H$_{23}$N$_5$O$_6$F$_2$Na: 478.1586, found: 478.15063 (M$^+$+Na).

4.8. 9-(3-Deoxy-3,4-difluoro-α-L-arabinofuranosyl)cytosine (19)

To a solution of **10** (119.3 mg, 0.31 mmol) in MeOH (5.0 mL) was added NaOMe (50.2 mg, 0.93 mmol) under Ar atmosphere at 0 °C and the mixture was stirred at rt for 12 h. The reaction mixture was neutralized with AcOH and chromatographed on silica gel (16% MeOH in CH_2Cl_2) to give **19** (76.7 mg, 94%) as a solid: mp, 103–106 °C; ^{1}H NMR (CD$_3$OD) δ 3.72–3.73 (2H, m, CH$_2$-5′), 4.64 (1H, dt, $J_{1',2'}$ = $J_{2',3'}$ = 7.4 and $J_{2',3'F}$ = 16.6 Hz, H-2′), 5.11 (1H, ddd, $J_{2',3'}$ = 7.4, $J_{3',4'F}$ = 17.5 and $J_{3',3'F}$ = 52.0 Hz, H-3′), 6.02 (1H, d, $J_{5,6}$ = 8.0 Hz, H-5), 6.27 (1H, t, $J_{1',2'}$ = $J_{1',4'F}$ = 7.4 Hz, H-1′), 7.66 (1H, d, $J_{5,6}$ = 8.0 Hz, H-6); ^{13}C NMR (CDCl$_3$) δ 60.8, 61.2, 76.6, 88.6, 88.7, 91.7, 91.9, 93.3, 93.5, 97.6, 141.76, 141.80, 158.4, 167.5; FAB-MS (m/z) 264 (M$^+$+H). Anal Calcd for C$_9$H$_{11}$F$_2$N$_3$O$_4$·

1/5MeOH·1/7Et$_2$O: C, 41.88; H, 4.65; N, 14.99. Found: C, 41.69; H, 4.55; N, 14.58.

4.9. 9-(3-Deoxy-3,4-difluoro-β-D-xylofuranosyl)cytosine (20)

To a solution of **11** (69.9 mg, 0.18 mmol) in MeOH (3.5 mL) was added NaOMe (29.2 mg, 0.54 mmol) and the mixture was stirred at rt for 12 h. The reaction mixture was neutralized with AcOH and chromatographed on silica gel (16% MeOH in CH$_2$Cl$_2$) to give **20** (42.7 mg, 90%) as a solid: mp, 92–94 °C; ^{1}H NMR (CD$_3$OD) δ 3.87 (1H, ddd, $J_{4'F,5'a}$ = 2.9, $J_{5'a,3'F}$ = 6.9 Hz and $J_{5'a,5'b}$ = 10.5 Hz, H-5'a), 3.90 (1H, dt, $J_{4'F,5'b}$ = $J_{3'F,5'b}$ = 2.9 and $J_{5'a,5'b}$ = 10.5 Hz, H-5'b), 4.42 (1H, dt, $J_{1',2'}$ = $J_{2',3'}$ = 3.4 and $J_{2',3'F}$ = 21.2 Hz, H-2'), 5.08 (1H, ddd, $J_{2',3'}$ = 2.3, $J_{3',4'F}$ = 6.9, $J_{3',3'F}$ = 49.8 Hz, H-3'), 5.97 (1H, d, $J_{5,6}$ = 7.4 Hz, H-5), 6.33 (1H, d, $J_{1',2'}$ = 3.4 Hz, H-1'), 7.58 (1H, d, $J_{5,6}$ = 7.4 Hz, H-6); ^{13}C NMR (CD$_3$OD) δ 61.6, 61.4, 79.0, 79.2, 93.28, 93.31, 97.2, 97.5, 97.9, 99.0, 99.3, 118.5, 118.8, 120.4, 120.6, 142.1, 158.0, 167.6; FAB-MS (*m/z*) 264 (M$^+$+H); Anal Calcd for C$_9$H$_{11}$F$_2$N$_3$O$_4$·0.9MeOH: C, 40.71; H, 4.72; N, 14.38. Found: C, 40.90; H, 4.65; N, 13.98.

4.10. 9-(3-Deoxy-3,4-difluoro-β-D-ribofuranosyl)cytosine (21)

To a solution of **12** (6.3 mg, 0.016 mmol) in MeOH (1.5 mL) was added NaOMe (2.6 mg, 0.048 mmol) at 0 °C under Ar atmosphere and the mixture was stirred at rt for 12 h. The reaction mixture was neutralized with AcOH and chromatographed on silica gel (16% MeOH in CH$_2$Cl$_2$) to give **21** (4.0 mg, 95%) as a solid: mp, 149–151 °C (dec); ^{1}H NMR (CD$_3$OD) δ 4.19 (1H, dd, $J_{4'F,5'a}$ = 3.4 and $J_{5'a,5'b}$ = 10.3 Hz, H-5'a), 4.23 (1H, dd, $J_{4'F,5'b}$ = 5.7 and $J_{5'a,5'b}$ = 10.3 Hz, H-5'b), 4.48 (1H, ddd, $J_{1',2'}$ = 3.4, $J_{2',3'}$ = 6.0 and $J_{2',3'F}$ = 7.2 Hz, H-2'), 5.23 (1H, ddd, $J_{2',3'}$ = 5.7, $J_{3',4'F}$ = 12.6 and $J_{3',3'F}$ = 51.0 Hz, H-3'), 5.89 (1H, d, $J_{5,6}$ = 7.4 Hz, H-5), 6.05 (1H, d, $J_{1',2'}$ = 3.4 Hz, H-1'), 7.73 (1H, d, $J_{5,6}$ = 7.4 Hz, H-6); ^{13}C NMR (CD$_3$OD) δ 62.3, 62.7, 72.6, 72.7, 95.2, 96.7, 129.9, 132.4, 143.9, 168.6; FAB-MS (*m/z*) 264 (M$^+$+H); Anal Calcd for C$_9$H$_{11}$F$_2$N$_3$O$_4$·0.7MeOH: C, 40.79; H, 4.87; N, 14.71. Found: C, 40.95; H, 4.62; N, 14.52.

4.11. 9-(3-Deoxy-3,4-difluoro-α-L-arabinofuranosyl)adenine (22)

To a solution of **15** (107.5 mg, 0.29 mmol) in MeOH (6.0 mL) was added K$_2$CO$_3$ (120.2 mg, 0.87 mmol) and the mixture was stirred at 0 °C under Ar atmosphere for 12 h. The reaction mixture was neutralized with AcOH and chromatographed on silica gel (8% MeOH in CH$_2$Cl$_2$) to give **22** (66.1 mg, 79%) as a solid: mp, 221–223 °C (dec); ^{1}H NMR (CD$_3$OD) δ 3.71 (1H, dd, $J_{4'F,5'a}$ = 5.7 and $J_{5'a,5'b}$ = 12.8 Hz, H-5'a), 3.75 (1H, dd, $J_{4'F,5'b}$ = 4.6 and $J_{5'a,5'b}$ = 12.8 Hz, H-5'b), 5.19 (1H, ddd, $J_{2',3'}$ = 7.7, $J_{3',4'F}$ = 43.1, and $J_{3',3'F}$ = 51.2 Hz, H-3'), 5.24 (1H, d, $J_{1',2'}$ = 6.3 and $J_{2',3'}$ = 7.7 Hz, H-2'), 6.16 (1H, t, $J_{1',2'}$ = $J_{1',4'F}$ = 6.3 Hz, H-1'), 8.22 and 8.31 (2H, each as s H-2 and H-8); ^{13}C NMR (CD$_3$OD) δ 60.8, 62.1, 76.6, 86.8, 86.9, 92.0, 92.2, 93.6, 93.8, 115.2, 115.3, 117.0, 117.2, 120.0, 140.3, 140.4, 151.2, 154.4, 157.5; FAB-MS (*m/z*) 288 (M$^+$+H). Anal Calcd for C$_{10}$H$_{11}$F$_2$N$_5$O$_3$·H$_2$O: C, 39.35; H, 4.29; N, 22.94. Found: C, 38.91; H, 4.64; N, 23.02.

4.12. 9-(3-Deoxy-3,4-difluoro-β-D-xylofuranosyl)adenine (23)

To a solution of **16** (17.1 mg, 0.046 mmol) in MeOH (6.0 mL) was added K$_2$CO$_3$ (120.2 mg, 0.87 mmol) and the mixture was stirred at 0 °C under Ar atmosphere for 12 h. The reaction mixture was neutralized with AcOH and chromatographed on silica gel (8% MeOH in CH$_2$Cl$_2$) to give **23** (10.8 mg, 82%) as a solid: mp, 194–196 °C; ^{1}H NMR (CD$_3$OD) δ 3.87 (1H, ddd, $J_{3'F,5'a}$ = 8.6 and $J_{4'F,5'a}$ =

$J_{5'a,5'b}$ = 12.9 Hz, H-5'a), 3.90 (1H, dt, $J_{3'F,5'b}$ = $J_{4'F,5'b}$ = 27.0 and $J_{5'a,5'b}$ = 12.9 Hz, H-5'b), 4.98 (1H, dt, $J_{1',2'}$ = $J_{2',3'}$ = 5.8 and $J_{2',3'F}$ = 14.5 Hz, H-2'), 5.21 (1H, ddd, $J_{2',3'}$ = 3.5, $J_{3',4'F}$ = 9.8, $J_{3',3'F}$ = 51.0 Hz, H-3'), 6.34 (1H, d, $J_{1',2'}$ = 4.6 Hz, H-1'), 8.22 and 8.23 (2H, each as s H-2 and H-8); ^{13}C NMR (CD$_3$OD) δ 61.5, 61.8, 63.0, 63.3, 72.1, 73.2, 78.4, 78.6,, 88.7, 88.9, 90.3, 91.3, 91.2, 98.1, 98.5, 99.6, 100.0, 120.4, 120.9, 140.8, 141.7, 150.3, 150.6, 154.0, 154,3, 157.6; FAB-MS (*m/z*) 288 (M$^+$+H). Anal Calcd for C$_{10}$H$_{11}$F$_2$N$_5$O$_3$·1/3H$_2$O: C, 40.96; H, 4.01; N, 23.88. Found: C, 40.72; H, 3.86; N, 23.78.

4.13. 9-(3-Deoxy-3,4-difluoro-β-D-ribofuranosyl)adenine (24)

To a solution of **17** (55.7 mg, 0.15 mmol) in MeOH (6.0 mL) was added K$_2$CO$_3$ (62.2 mg, 0.45 mmol) and the mixture was stirred at 0 °C under Ar atmosphere for 12 h. The reaction mixture was neutralized with AcOH and chromatographed on silica gel (8% MeOH in CH$_2$Cl$_2$) to give **24** (36.7 mg, 85%) as a solid: mp, 187–189 (dec) °C; ^{1}H NMR (CD$_3$OD) δ 3.79–3.80 (2H, m, CH$_2$-5'), 4.99 (1H, dt, $J_{1',2'}$ = $J_{2',3'}$ = 5.8 and $J_{2',3'F}$ = 14.5 Hz), 5.43 (1H, ddd, $J_{2',3'}$ = 5.8, $J_{3',4'F}$ = 35.8, $J_{3',3'F}$ = 52.0 Hz, H-3'), 6.32 (1H, d, $J_{1',2'}$ = 5.8 Hz, H-1'), 8.19 and 8.28 (2H, each as s H-2 and H-8); ^{13}C NMR (CD$_3$OD) δ 63.1, 63.4, 73.1, 73.3, 88.8, 88.9, 90.3, 90.5, 91.2, 97.3, 115.6, 115.8, 117.5, 117.7, 120.9, 141.7, 150.3, 154.0, 157.6; FAB-MS (*m/z*) 288 (M$^+$+H). Anal Calcd for C$_{10}$H$_{11}$F$_2$N$_5$O$_3$·H$_2$O: C, 39.35; H, 4.29; N, 22.94. Found: C, 38.98; H, 4.13; N, 23.10.

4.14. 9-(3-Deoxy-3,4-difluoro-α-L-xylofuranosyl)adenine (25)

To a solution of **18** (8.2 mg, 0.022 mmol) in MeOH (2.0 mL) was added K$_2$CO$_3$ (9.1 mg, 0.066 mmol) and the mixture was stirred at 0 °C under Ar atmosphere for 12 h. The reaction mixture was neutralized with AcOH and chromatographed on silica gel (8% MeOH in CH$_2$Cl$_2$) to give **25** (5.4 mg, 84%) as a solid: mp, 205–207 °C (dec); ^{1}H NMR (CD$_3$OD) δ 3.71 (1H, dd, $J_{4'F,5'a}$ = 5.7 and $J_{5'a,5'b}$ = 12.8 Hz, H-5'a), 3.75 (1H, dd, $J_{4'F,5'b}$ = 4.6 and $J_{5'a,5'b}$ = 12.8 - Hz, H-5'b), 5.19 (1H, ddd, $J_{2',3'}$ = 7.7, $J_{3',4'F}$ = 43.1, and $J_{3',3'F}$ = 51.2 Hz, H-3'), 5.24 (1H, d, $J_{1',2'}$ = 6.3 and $J_{2',3'}$ = 7.7 Hz, H-2'), 6.16 (1H, t, $J_{1',2'}$ = $J_{1',4'F}$ = 6.3 Hz, H-1'), 8.22 and 8.31 (2H, each as s H-2 and H-8); ^{13}C NMR (CD$_3$OD) δ 61.0, 61.2, 74.0, 74.2, 91.2, 91.6, 92.7, 93.1, 118.9, 120.2, 120.5, 140.5, 151.4, 154.4, 157.5; FAB- MS (*m/z*) 288 (M$^+$+H). Anal Calcd for C$_{10}$H$_{11}$F$_2$N$_5$O$_3$·1/2H$_2$O: C, 40.55; H, 4.08; N, 23.64. Found: C, 40.79; H, 3.81; N, 24.01.

4.15. RL assay for anti-HCV activity[21]

The OR6 cells were plated onto 24-well plates (2 × 10^4 cells per well) in triplicate and then treated with each reagent at several concentrations for 72 h. After treatment, the cells were subjected to luciferase assay using the RL assay system (Promega, Madison, WI). In several cases, the 50% effective concentration (EC$_{50}$) was determined. The value of selective index (SI) was determined by dividing the CC$_{50}$ value by the EC$_{50}$ value.

4.16. WST-1 cell proliferation assay for cytotoxicity[22]

Using ORL8 cells, we first performed WST-1 cell proliferation assay at three or four different concentrations to determine the concentration of compounds for the assay of anti-HCV activity. The cells were plated onto 96-well plates (1 × 10^3 cells per well) in triplicate and then treated with each reagent at three or four concentrations for 72 h. After treatment, the cells were subjected to the WST-1 cell proliferation assay (Takara Bio, Otsu, Japan) according to the manufacturer's protocol. From the assay results, we chose the concentration showing the relative activity of

approximately 80% as a maximum concentration for the assay of anti-HCV activity. In several cases, the 50% cytotoxic concentration (CC_{50}) was determined.

Acknowledgments

References and notes

1. *Nucleosides and Nucleotides as Antitumor and Antiviral Agents*; Chu, C. K., Baker, D. C., Eds.; Plenum Press: New York, 1993.
2. Ichikawa, E.; Kato, K. *Curr. Med. Chem.* **2001**, *8*, 385.
3. *Modified Nucleosides in Biochemistry, Biotechnology and Medicine*; Herdewijn, P., Ed.; Wiley-VCH: Weinheim, 2008.
4. *Chemical Synthesis of Nucleoside Analogues*; Merino, P., Ed.; John Wiley & Sons: Hoboken, New Jersey, 2013.
5. (a) Gui, X.-L.; Xu, X.-H.; Qing, F.-L. *Tetrahedron* **2010**, *66*, 789. and references cited therein; (b) Sofia, M. J.; Bao, D.; Chang, W.; Du, J.; Nagarathnam, D.; Rachakonda, S.; Reddy, P. G.; Ross, B. S.; Wang, P.; Zhang, H. R.; Bansal, S.; Espiritu, C.; Keilman, M.; Lam, A. M.; Syeuer, H. M.; Niu, C.; Otto, M. J.; Furman, P. A. *J. Med. Chem.* **2010**, *53*, 7202.
6. Jeong, L. S.; Marques, V. E. *J. Org. Chem.* **1995**, *60*, 4276. and references cited therein.
7. Marques, V. E.; Lin, B. B.; Barchi, J. J., Jr.; Nicklaus, M. C. Nucleosides and Nucleotides as Antitumor and Antiviral Agents In Chu, C. K., Baker, D. C., Eds.; Plenum Press: New York, 1993; pp 265–284.
8. Kubota, Y.; Ehara, M.; Haraguchi, K.; Tanaka, H. *J. Org. Chem.* **2011**, *76*, 8710. and references cited therein.
9. Haraguchi, K.; Itoh, Y.; Tanaka, H. *J. Synth. Org. Chem. Jpn.* **2003**, *61*, 974.
10. Haraguchi, K.; Tanaka, H.; Itoh, Y.; Miyasaka, T. *J. Org. Chem.* **1996**, *61*, 851.
11. Filler, R. *Isr. J. Chem.* **1978**, *17*, 71.
12. Gergorcic, A.; Zupan, M. *J. Org. Chem.* **1979**, *44*, 4120.
13. Korytnyk, W.; Valentekovic-Horvath, S. *Tetrahedron Lett.* **1980**, 1493.
14. Korytnyk, W.; Valentekovic-Horvath, S.; Petrie, C. R., III *Tetrahedron* **1982**, *38*, 2547.
15. Hall, L. H.; Steiner, P. R.; Pedersen, C. *Can. J. Chem.* **1970**, *48*, 1155.
16. Bock, K.; Pedersen, C.; Wiebe, L. *Acta Chem. Scand.* **1973**, *27*, 3586.
17. Kubota, Y.; Haraguchi, K.; Kunikata, M.; Hayashi, M.; Ohkawa, M.; Tanaka, H. *J. Org. Chem.* **2006**, *71*, 1099.
18. Saenger, W. *Principles of Nucleic Acid Structure*; Springer: New York Berlin, Heidelberg, Tokyo, 1984.
19. Karthe, P.; Gautham, N.; Kumar, A.; Katti, S. B. *Acta Cryst.* **1997**, *C53*, 1694.
20. Barchi, J. J., Jr.; Karki, R. G.; Nicklaus, M. C.; Siddiqui, M. A.; George, C.; Mikhailopulo, I. A.; Marquez, V. *J. Am. Chem. Soc.* **2008**, *130*, 9048. and references cited therein.
21. Kato, N.; Mori, K.; Abe, K.; Dansako, H.; Kuroki, M.; Ariumi, Y.; Wakita, T.; Ikeda, M. *Virus Res.* **2009**, *146*, 41.
22. Ueda, Y.; Mori, K.; Ariumi, Y.; Ikeda, M.; Kato, N. *Biochem. Biophys. Res. Commun.* **2011**, *409*, 663.
23. Eldrup, D. B.; Martin, J. A.; Klumpp, K.; Baker, S. J.; Blomgren, P. A.; Devos, R.; Granycome, A. B.; Allerson, C. R.; Bennett, C. F.; Bera, S.; Bhat, B.; Bhat, N.; Bosserman, M. R.; Brooks, J.; Burlein, C.; Carroll, S. S.; Cook, P. D.; Getty, K. L.; MacCoss, M.; McMasters, D. R.; Olsen, D. B.; Prakash, T. P.; Prhavc, M.; Song, Q.; Tomassini, J. E.; Xia, J. *J. Med. Chem.* **2004**, *47*, 2283.

ELSEVIER

GASTROINTESTINAL, HEPATOBILIARY, AND PANCREATIC PATHOLOGY

Hepatitis C Virus Core Protein Suppresses Mitophagy by Interacting with Parkin in the Context of Mitochondrial Depolarization

Yuichi Hara,* Izumi Yanatori,[†] Masanori Ikeda,[‡] Emi Kiyokage,[§] Sohji Nishina,* Yasuyuki Tomiyama,* Kazunori Toida,[§] Fumio Kishi,[†] Nobuyuki Kato,[‡] Michio Imamura,[¶] Kazuaki Chayama,[¶] and Keisuke Hino*

From the Departments of Hepatology and Pancreatology,* Molecular Genetics,[†] and Anatomy,[§] Kawasaki Medical School, Kurashiki; the Department of Tumor Virology,[‡] Okayama University Graduate School of Medicine, Dentistry and Pharmaceutical Sciences, Okayama; and the Department of Gastroenterology and Metabolism,[¶] Applied Life Sciences, Institute of Biomedical and Health Sciences, Hiroshima University, Hiroshima, Japan

Hepatitis C virus (HCV) causes mitochondrial injury and oxidative stress, and impaired mitochondria are selectively eliminated through autophagy-dependent degradation (mitophagy). We investigated whether HCV affects mitophagy in terms of mitochondrial quality control. The effect of HCV on mitophagy was examined using HCV-Japanese fulminant hepatitis-1—infected cells and the uncoupling reagent carbonyl cyanide m-chlorophenylhydrazone as a mitophagy inducer. In addition, liver cells from transgenic mice expressing the HCV polyprotein and human hepatocyte chimeric mice were examined for mitophagy. Translocation of the E3 ubiquitin ligase Parkin to the mitochondria was impaired without a reduction of pentaerythritol tetranitrate—induced kinase 1 activity in the presence of HCV infection both in vitro and in vivo. Coimmunoprecipitation assays revealed that Parkin associated with the HCV core protein. Furthermore, a Yeast Two-Hybrid assay identified a specific interaction between the HCV core protein and an N-terminal Parkin fragment. Silencing Parkin suppressed HCV core protein expression, suggesting a functional role for the interaction between the HCV core protein and Parkin in HCV propagation. The suppressed Parkin translocation to the mitochondria inhibited mitochondrial ubiquitination, decreased the number of mitochondria sequestered in isolation membranes, and reduced autophagic degradation activity. Through a direct interaction with Parkin, the HCV core protein suppressed mitophagy by inhibiting Parkin translocation to the mitochondria. This inhibition may amplify and sustain HCV-induced mitochondrial injury. *(Am J Pathol 2014, 184: 3026—3039; http://dx.doi.org/10.1016/j.ajpath.2014.07.024)*

Oxidative stress is present in chronic hepatitis C to a greater degree than in other inflammatory liver diseases.[1,2] The hepatitis C virus (HCV) core protein induces the production of reactive oxygen species (ROS)[3,4] through mitochondrial electron transport inhibition.[5] Because the mitochondria are targets for ROS and ROS generators, HCV-induced ROS have the potential to injure mitochondria. In addition, hepatocellular mitochondrial alterations have been observed in patients with chronic hepatitis C.[6] We previously identified a ROS-associated iron metabolic disorder[7] and demonstrated that transgenic mice expressing the HCV polyprotein develop hepatocarcinogenesis related to mitochondrial injury induced by HCV and iron overload.[8] Therefore, impaired mitochondrial function may play a critical role in

the development of hepatocellular carcinoma (HCC) in patients with chronic HCV infection. Conversely, the affected mitochondria are selectively eliminated through the autophagy-dependent degradation of mitochondria (referred to as mitophagy) in both physiological and pathological settings to maintain the mitochondrial quality.[9,10] On the

basis of these observations, we hypothesized that HCV may suppress mitophagy, which could lead to the sustained presence of affected mitochondria, increased ROS production, and the development of HCC.

Mitochondrial membrane depolarization precedes mitophagy induction,[11] which is selectively controlled by a variety of proteins in mammalian cells, including pentaerythritol tetranitrate—induced kinase 1 (PINK1) and the E3 ubiquitin ligase Parkin.[12—19] PINK1 facilitates Parkin targeting of the depolarized mitochondria.[12—15] Although Parkin ubiquitinates a broad range of mitochondrial outer membrane proteins,[14,17—19] it remains unclear how Parkin enables the damaged mitochondria to be recognized by the autophagosome. Structures containing autophagy-related protein 9A and the uncoordinated family member-51—like kinase 1 complex independently target depolarized mitochondria at the initial stages of Parkin-mediated mitophagy, whereas the autophagosomal microtubule-associated protein light chain 3 (LC3) is critical for efficient incorporation of damaged mitochondria into the autophagosome at a later stage.[20] LC3-I undergoes post-translational modification by phosphatidylethanolamine to become LC3-II, and LC3-II insertion into the autophagosomal membrane is a key step in autophagosome formation. In addition, the autophagic adaptor p62 is recruited to mitochondrial clusters and is essential for mitochondrial clearance,[13] although it remains controversial as to whether p62 is essential for mitochondrial recognition by the autophagosome[13] or rather is important for perinuclear clustering of depolarized mitochondria.[19-21] Our aim was to examine whether HCV suppresses mitophagy. We found that HCV core protein inhibits the translocation of Parkin to affected mitochondria by interacting with Parkin and subsequently suppressing mitophagy. These results imply that mitochondria affected by HCV core protein are unlikely to be eliminated, which may intensify oxidative stress and increase the risk of hepatocarcinogenesis.

Materials and Methods

Cell Culture, HCV Infection Experiments, and Mitochondrial Depolarization

HCV-Japanese fulminant hepatitis-1 (JFH1)—infected Huh7 cells have previously been described in detail.[22] The supernatants were collected from cell culture—generated JFH1-Huh7 cells at 21 days after infection and stored until use at −80°C after filtering through a 0.45-μm filter. For infection experiments with the HCV-JFH1 virus, 1×10^5 Huh7 cells per well were plated onto 6-well plates and cultured for 24 hours. Then, we infected the cells with 50 μL (equivalent to a multiplicity of infection of 0.1) of inoculum. The culture supernatants were collected, and the levels of the HCV core were determined using an enzyme-linked immunosorbent assay (ELISA; Mitsubishi Kagaku Bio-Clinical Laboratories, Tokyo, Japan). Total RNA was isolated from the infected cellular lysates using an RNeasy mini kit (Qiagen, Hilden, Germany) for quantitative

RT-PCR analysis of the intracellular HCV RNA. The HCV infectivity in the culture supernatants was determined by a focus-forming assay at 48 hours after infection. The HCV-infected cells were detected using an anti-HCV core antibody (CP-9 and CP-11, Institute of Immunology, Ltd, Tokyo, Japan). Intracellular HCV infectivity was determined using a focus-forming assay at 48 hours after inoculation of the lysates by repeated freeze-and-thaw cycles (three times).

To depolarize the mitochondria, the cells were treated with 10 μmol/L carbonyl cyanide m-chlorophenylhydrazone (CCCP; Sigma-Aldrich, St. Louis, MO) for 1 to 2 hours or 1 μmol/L valinomycin (Sigma-Aldrich) for 3 hours; CCCP represses ATP synthesis through the loss of the H^+ gradient without affecting mitochondrial electron transport, which is known to induce mitochondrial fragmentation.[13]

Animals

The pAlbSVPA-HCV vector, which contains the full-length polyprotein-coding region under the control of the murine albumin promoter/enhancer, has previously been described in detail.[23,24] Of the four transgenic lineages with evidence of RNA transcription of the full-length HCV-N open reading frame (FL-N), the FL-N/35 lineage proved capable of breeding large numbers.[24] Urokinase-type plasminogen activator—transgenic severe combined immunodeficiency mice were generated, and human hepatocytes were transplanted to generate chimeric mice.[25] The chimeric mice were injected with genotype *1b* HCV-positive human serum samples, as described previously.[26] The mouse livers were extracted 12 weeks after the infection, when the serum HCV RNA titers had increased over baseline levels. Male FL-N/35 transgenic mice, age-matched C57BL/6 mice (control), and chimeric mice with and without HCV infection were fed, maintained, and then euthanized by i.p. injection of 10% nembutal sodium, according to the guidelines approved by the Institutional Animal Care and Use Committee. The study protocol for obtaining human serum samples conformed to the ethical guidelines of the 1975 Declaration of Helsinki and was approved by the Institutional Review Committee.

Measurement of HCV RNA and Human Albumin in the Serum of Chimeric Mice

HCV RNA[26] and human albumin[25] were quantified as described previously. Human albumin levels in the serum of chimeric mice were determined using the Human Albumin ELISA Quantification kit (Bethyl Laboratories Inc., Montgomery, TX).

Measurement of Mitochondrial Membrane Potential

The mitochondrial membrane potential ($\Delta\Psi$) was measured using a Cell Meter JC-10 Mitochondrial Membrane Potential Assay kit (AAT Bioquest, Inc., Sunnyvale, CA), according to the manufacturer's instructions. The fluorescent intensities

for both J-aggregates (red) and monometric forms (green) of JC-10 were measured at Ex/Em = 490/525 nm and 540/590 nm with a Varioskan Flush Multimode Reader (Thermo Fisher Scientific, Waltham, MA).

Isolation of Mitochondria

The cells were lysed by mechanical homogenization using a small pestle, and mitochondrial extraction was performed using a Qproteome Mitochondria Isolation kit (Qiagen), according to the manufacturer's instructions. Liver mitochondria were isolated as described previously with some modifications.[27] In brief, the livers were minced on ice and homogenized by five strokes with a Dounce homogenizer and a tight-fitting pestle in isolation buffer [70 mmol/L sucrose, 1 mmol/L KH_2PO_4, 5 mmol/L HEPES, 220 mmol/L mannitol, 5 mmol/L sodium succinate, and 0.1% bovine serum albumin (BSA), pH 7.4]. The homogenate was centrifuged at 800 × g for 5 minutes at 4°C. The supernatant fraction was retained, whereas the pellet was washed with isolation buffer and centrifuged again. The combined supernatant fractions were centrifuged at 1000 × g for 15 minutes at 4°C to obtain a crude mitochondrial pellet.

Measurement of ROS

The cellular ROS level was measured by oxidation of the cell-permeable, oxidation-sensitive fluorogenic precursor, 2',7'-dihydrodichlorofluorescein diacetate (Molecular Probes Inc., Eugene, OR). Fluorescence was measured using a Varioskan Flush Multimode Reader at 495/535 nm (excitation/emission).

Determination of Glutathione Content

Mitochondrial pellets were measured for total glutathione [reduced glutathione (GSH) + oxidized glutathione (GSSG)] and GSH content using the GSSG/GSH Quantification kit (Dojindo Molecular Technologies, Inc., Kumamoto, Japan). The concentration of GSH was calculated using the following formula:

$$\text{GSH concentration} = \text{Total glutathione concentration}$$
$$- [\text{GSSG concentration}] \times 2 \qquad (1)$$

The liver tissue samples (approximately 50 mg) were minced in ice-cold metaphosphoric acid solution, homogenized, and centrifuged at 3000 × g for 10 minutes at 4°C. Lysates from the liver tissue samples and mitochondrial samples (2 mg) were evaluated for the concentration of GSH using the thioester method and a GSH-400 kit (Oxis International Inc., Portland, OR) and for total glutathione content using the glutathione reductase—dinitrothiocyanobenzene recycling assay and the GSH-412 kit (Oxis International Inc.), as described previously.[5]

Immunoblotting

Samples were lysed in radioimmunoprecipitation assay buffer [20 mmol/L Tris-HCl (pH 7.5), 150 mmol/L NaCl,

50 mmol/L NaF, 1 mmol/L Na_3VO_4, 0.1% SDS, and 0.5% Triton X-100], as described previously,[28] supplemented with 1% protease inhibitor mixture (Sigma-Aldrich) and 100 mmol/L phenylmethylsulfonyl fluoride. Cell lysates or mitochondrial pellets were subjected to immunoblot analysis using an iBlot Gel Transfer Device (Invitrogen, Carlsbad, CA). The membranes were incubated with the following primary antibodies: rabbit anti-human LC3 (Novus Biologicals, Littleton, CO), rabbit anti-human p62/SQSTM1 (MBL, Nagoya, Japan), rabbit anti-human Parkin (Cell Signaling Technology, Danvers, MA), mouse anti-human Parkin (Santa Cruz Biotechnology, Inc.), rabbit anti-human p-Parkin (Ser 378; Santa Cruz Biotechnology, Inc.), rabbit anti-human PINK1 (Cell Signaling Technology), mouse anti-human mitochondrial heat shock protein-70 (BioReagents, Golden, CO), mouse anti-human ubiquitin (Santa Cruz Biotechnology, Inc.), goat anti-human voltage-dependent anion-selective channel protein 1 (VDAC1; Santa Cruz Biotechnology, Inc.), monoclonal antisynthetic HCV core peptide (CP11; Institute of Immunology, Ltd), mouse anti-HCV non-structural (NS) 3 protein (Abcam, Cambridge, MA), mouse anti-HCV NS4A (Abcam), mouse anti-HCV NS5A protein (Abcam), and rabbit anti-human β-actin (Cell Signaling Technology).

Electron Microscopy

To address the detail localization of core and Parkin, the cells treated with CCCP for 1 hour were fixed with 4% paraformaldehyde and 1% glutaraldehyde in 0.1 mol/L Millonig's phosphate buffer (pH 7.4) for 30 minutes. The cells were incubated with a mixture of the following primary antibodies in phosphate-buffered saline (PBS) containing 1% BSA and 0.05% sodium azide overnight at 20°C: mouse monoclonal antisynthetic HCV core peptide (Institute of Immunology), rabbit anti-human Parkin (Abcam), and rabbit anti-rat LC3 (Wako Pure Chemical Industries, Ltd, Osaka, Japan). After washing with PBS, the cells were incubated with biotinylated donkey anti-rabbit IgG (Jackson ImmunoResearch Laboratories, Inc., Baltimore Pike, PA) in 1% BSA for 2 hours at 20°C. After washing with PBS, the cells were incubated with Alexa Fluor-488 FluoroNanogold-streptavidin (Jackson ImmunoResearch Laboratories, Inc.), indocarbocyanine-labeled donkey anti-mouse IgG (Jackson ImmunoResearch Laboratories, Inc.), and indocarbocyanine-labeled donkey anti-rabbit IgG (Jackson ImmunoResearch Laboratories, Inc.) in 1% BSA for 2 hours at 20°C. After washing with PBS, the cells were incubated with mouse peroxidase—anti-peroxidase complex (Jackson ImmunoResearch Laboratories, Inc.) in PBS for 3 hours at 20°C. The peroxidase reduction was developed with 0.05% diaminobenzidine tetrahydrochloride in 50 mmol/L Tris buffer containing 0.01% hydrogen peroxide for 20 minutes at room temperature. The diameter of the gold immunoparticles was increased using a silver enhancement kit (HQ silver; Nanoprobes, Inc., Yaphank, NY) for 4 minutes at

room temperature. After treatment with 1% osmium and 2% uranyl acetate, the cells were dehydrated in a graded series of ethanol and embedded in Epon-Araldite (OKEN, Tokyo, Japan). Serial ultrathin sections (each 70 nm thick) were examined using an electron microscope (model JEM1400; JEOL, Tokyo, Japan). These immune—electron microscopic methods were generally performed according to our previous study.[29]

Immunofluorescence Microscopy

The cells were fixed, permeabilized, and immunostained with rabbit anti-human Parkin (Abcam), goat anti-human Parkin (Santa Cruz Biotechnology, Inc.), goat anti-human Tom20 (Santa Cruz Biotechnology, Inc.), rabbit anti-rat LC3 (Wako Pure Chemical Industries, Ltd), or mouse monoclonal anti-synthetic HCV core peptide (Institute of Immunology) antibodies, followed by Cy3-conjugated donkey anti-rabbit IgG (Jackson ImmunoResearch Laboratories, Inc.), fluorescein isothiocyanate—conjugated donkey anti-goat IgG (Jackson ImmunoResearch Laboratories, Inc.), or Alexa Fluor 647—conjugated donkey anti-mouse IgG (Jackson ImmunoResearch Laboratories, Inc.). Cell images were captured using a confocal microscope (model LSM700; Zeiss, Jena, Germany) equipped with 488-, 555-, and 639-nm diodes. The images were acquired in a sequential mode using a 63× Plan Apochromat numerical aperture/1.4 oil objective and the appropriate filter combinations. All images were saved as tagged image file format files. The contrast was adjusted using Photoshop version CS5 (Adobe, San Jose, CA), and the images were imported into Illustrator version CS5 (Adobe). Colocalization was assessed with line scans using ImageJ software version 1.46 (NIH, Bethesda, MD).

Coimmunoprecipitation

Coimmunoprecipitation was performed using a Dynabeads Co-Immunoprecipitation Kit (Invitrogen), according to the manufacturer's instructions. Magnetic beads (Dynabeads M-270 Epoxy) were conjugated to anti-VDAC1 (Santa Cruz Biotechnology, Inc.), anti-Parkin (Cell Signaling Technology), anti-ubiquitin (Santa Cruz Biotechnology, Inc.), or anti-p62 (MBL) antibodies by rotating overnight at 37°C. The antibody-Dynabeads complex was then treated with coupling buffer. Beads coupled to anti-VDAC, anti-Parkin, anti-ubiquitin, or anti-p62 were incubated with cell lysates for 30 minutes at 4°C and then washed with coupling buffer. Collected protein complexes were subjected to immunoblot analysis using anti-VDAC, anti-ubiquitin (Santa Cruz Biotechnology, Inc.), and anti-Parkin (Cell Signaling Technology) antibodies to detect coimmunoprecipitated VDAC1, ubiquitin, and Parkin. Immunoblots using anti-Parkin, anti-HCV core (Institute of Immunology), anti-HCV NS3 (Abcam), anti-HCV NS4A (Abcam), or anti-HCV NS5A (Abcam) antibodies were performed to detect the coimmunoprecipitation of Parkin with core, NS3, NS4A, or NS5A protein.

RNA Interference

The siRNA knockdown oligonucleotides were obtained from Invitrogen. JFH1-Huh7 cells and/or Huh7 cells were grown to 50% to 60% confluency and transfected with 100 pmol siRNA oligonucleotides [5′-GGACGCUGUUCCUCGUUAUGAA-GAA-3′ (forward) and 5′-UUCUUCAUAACGAGGAACA-GCGUCC-3′ (reverse)] for PINK1 or siRNA oligonucleotides [5′-UCCAGCUCAAGGAGGUGGUUGCUAA-3′ (forward) and 5′-UUAGCAACCACCUCCUUGAGCUGGA-3′ (reverse)] for Parkin using Lipofectamine 2000 (Invitrogen). The cells were analyzed 72 hours after transfection.

Yeast Two-Hybrid Assay

A Matchmaker Gal4 two-hybrid system 3 (Clontech Laboratories, Inc., Mountain View, CA) was used according to the manufacturer's instructions. *Saccharomyces cerevisiae* Y187, containing an N- or C-terminal fragment cDNA of Parkin as a prey cloned into the Gal4-activation domain vector (pACT2), was allowed to mate with *S. cerevisiae* AH109, which had been transformed with a Gal4 DNA-binding domain vector (pGBKT7) containing the HCV core as bait. In addition, *S. cerevisiae* Y187, with the HCV core as a prey cloned into the Gal4-activation domain vector (pACT2), was allowed to mate with *S. cerevisiae* AH109, which had been transformed with a Gal4 DNA-binding domain vector (pGBKT7) containing N- or C-terminal fragment cDNA of Parkin as bait. To construct the prey and the bait, two regions of the Parkin gene that encoded the N-terminal 215—amino acid residues (1 to 215) and the C-terminal 250—amino acid residues (216 to 465) were amplified using PCR with genomic cDNA, and the HCV core gene was amplified with the HCV-O (genotype *1b*) genomic cDNA.[30] The PCR primers were as follows with the incorporated BamHI and EcoRI sites underlined: Parkin 1 to 215, 5′-<u>GGATCC</u>GCATGATAGTGTTTGTCAGGTT-3′ (forward) and 5′-<u>GAATTC</u>CTAGTGTGCTCCACATTTAA-AGA-3′ (reverse); Parkin 216 to 465, 5′-<u>GGATCC</u>GCCC-CACCTCTGACAAGGAAAC-3′ (forward) and 5′-<u>GAAT-TCC</u>TACACGTCGAACCAGTGGT-3′ (reverse); and HCV core, 5′-<u>GAATTC</u>GCCATGAGCACAAATCCTAAACCT-C-3′ (forward) and 5′-<u>GGATCC</u>TTAAGCGGAAGCTGG-GATGGTCAAA-3′ (reverse).

Real-Time RT-PCR

Total RNA was extracted from frozen liver tissues and cells using the RNeasy mini kit (Qiagen). Total RNA (2 μg) was reverse transcribed to cDNA using the High-Capacity RNA to cDNA kit (Applied Biosystems, Foster City, CA), according to the manufacturer's instructions. TaqMan Gene Expression Assays for LC3B, glyceraldehyde-3-phosphate dehydrogenase (GAPDH), Parkin, and HCV core were purchased from Applied Biosystems, and mRNA levels were quantified in triplicate using an Applied Biosystems

Statistical Analysis

Quantitative values are expressed as the means ± SD. Data were compared between the two groups using the Student's t-test. $P < 0.05$ was considered significant.

Results

Mitochondrial Oxidative Status *in Vitro* and *in Vivo*

After treatment with CCCP, a widely adopted reagent for inducing mitophagy, the mitochondrial membrane potential ($\Delta\Psi$) was significantly reduced irrespective of HCV infection (Figure 1A). The ratio of reduced/total glutathione content was decreased in the mitochondrial fraction after CCCP treatment in JFH1-Huh7 cells (Figure 1B). Thus, the mitochondrial oxidative status after CCCP treatment was present in HCV-infected cells (JFH1-Huh7). The ratio of reduced/total glutathione content was also decreased in the mitochondrial fraction but not in the whole liver in transgenic mice and HCV-infected chimeric mice compared with the control mice (Figure 1, C and D). These results suggest that there is a baseline oxidation level within the mitochondrial glutathione pool in these transgenic mice and HCV-infected chimeric mice. Furthermore, the mitochondria in these transgenic mice and HCV-infected chimeric mice can undergo mitophagy.

Impaired Recruitment of Parkin to the Mitochondria

Parkin phosphorylation and translocation to the mitochondria after CCCP treatment are indispensable for mitochondrial ubiquitination and subsequent autophagosome formation during the course of mitophagy.[13,15] CCCP exposure induced Parkin accumulation in the mitochondria of Huh7 cells; however, this Parkin recruitment seemed to be inhibited in JFH1-Huh7 cells (Figure 2A). CCCP treatment induces mitochondrial fission, followed by mitophagy.[13] CCCP-treated Huh7 cells displayed fragmented mitochondria colocalized with Parkin, except for a few mitochondrial tubular network cells. Western blot analysis also showed that CCCP-induced recruitment of Parkin to the mitochondria was suppressed without any change in Parkin expression or phosphorylation levels in whole cell lysates of JFH1-Huh7 cells (Figure 2B). Neither CCCP treatment nor HCV infection significantly increased the mRNA levels of Parkin in Huh7 cells, even though there was a tendency of increase in Parkin mRNA after HCV infection (Figure 2C). These results indicate that HCV infection could inhibit Parkin recruitment to CCCP-induced depolarized mitochondria.

The unique and high concentration of CCCP (10 μmol/L) used in the present study may have affected cellular functions
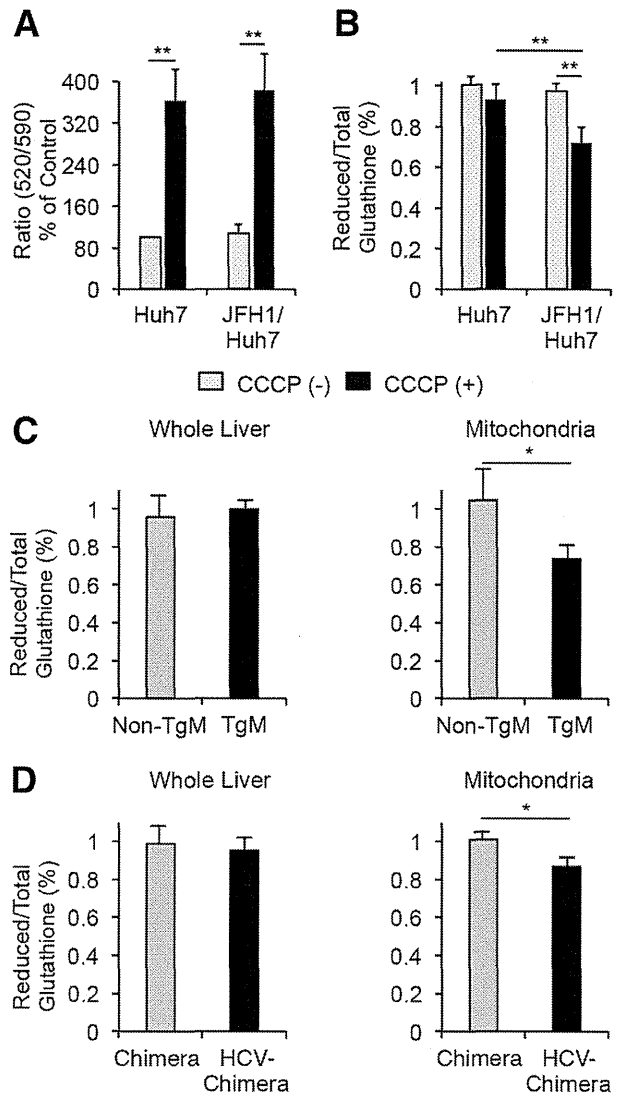
Figure 1 Mitochondrial membrane potential ($\Delta\Psi$) and glutathione content. **A:** Changes in $\Delta\Psi$ levels after a 1-hour carbonyl cyanide *m*-chlorophenylhydrazone (CCCP) treatment for Huh7 and JFH1-Huh7 cells ($n = 5$). The *y* axis represents the ratio of red (JC-10 aggregate form)/green (JC-10 monometric form) fluorescence intensity. **B:** Reduced and total glutathione content in mitochondrial fractions ($n = 5$). Reduced glutathione content was normalized to total glutathione content. Reduced and total glutathione content of freshly isolated whole liver homogenates or mitochondrial fractions of transgenic livers ($n = 7$, **C**) or HCV-infected chimeric mice livers ($n = 5$, **D**) compared with the content in the corresponding control liver samples. Reduced glutathione content was normalized to total glutathione content. *$P < 0.05$, **$P < 0.01$.

other than the proton gradient,[31] which suggests that Parkin translocation from the cytoplasm to the mitochondria may not be induced specifically through mitochondrial depolarization. Therefore, we examined mitochondrial accumulation of Parkin using lower CCCP concentrations (0.1, 1, 5, or 10 μmol/L). In coimmunoprecipitation experiments, CCCP exposure induced ubiquitinated Parkin accumulation in the mitochondria in a dose-dependent manner in Huh7 cells, as described previously,[13] but did not induce these changes in JFH1-Huh7 cells (Figure 2D). These results suggest that
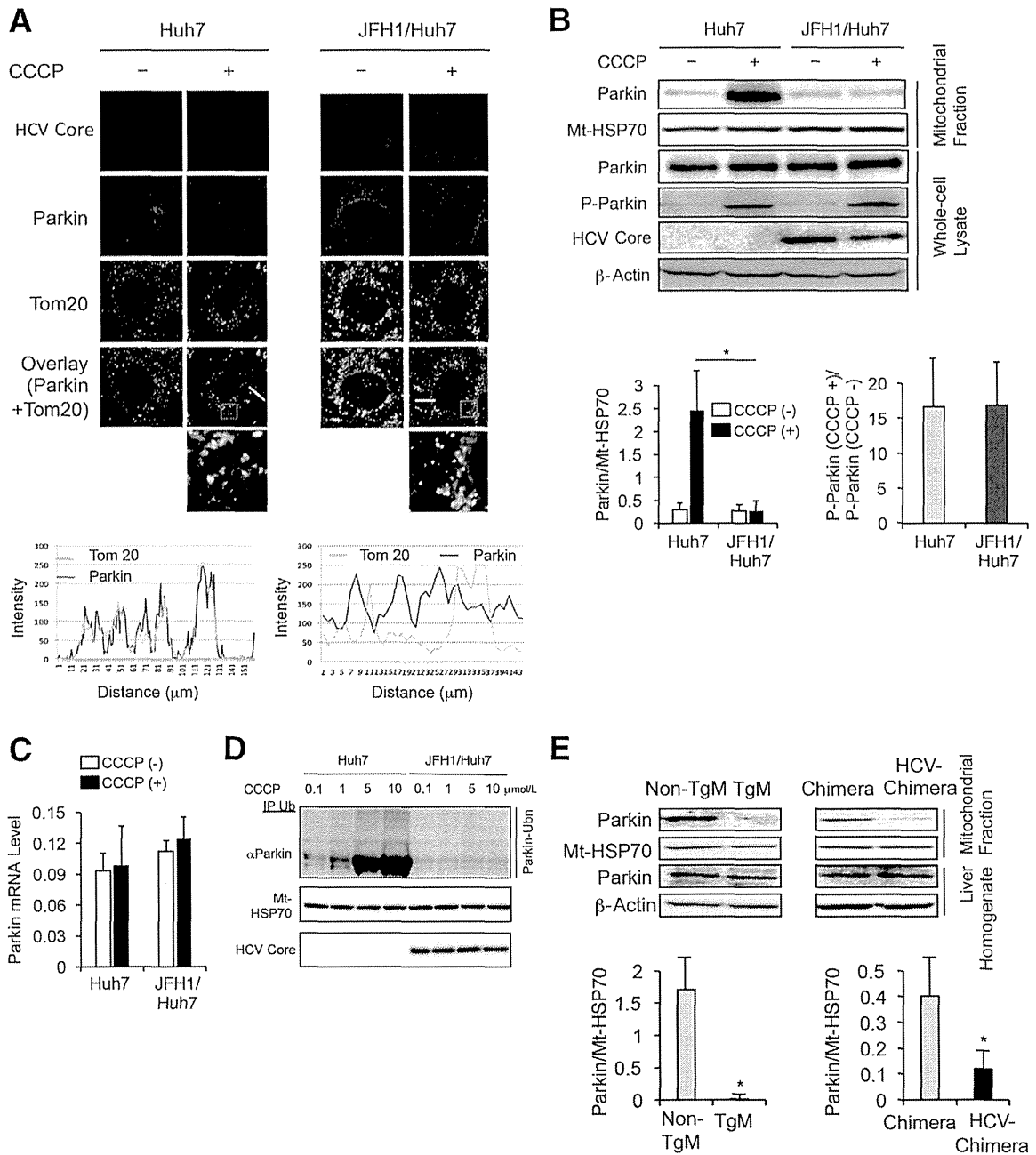
Figure 2 Effect of HCV on the translocation of Parkin to the mitochondria. **A:** Immunofluorescence staining for Parkin (red) and the mitochondrial marker Tom20 (green) in Huh7 and JFH1-Huh7 cells before (−) and after (+) carbonyl cyanide m-chlorophenylhydrazone (CCCP) treatment for 1 hour. **Boxed areas** are enlarged below. Endogenous Parkin that colocalizes with the mitochondria (yellow spots). Line scans indicate the colocalization of Parkin with the mitochondria and correlate to the **white lines** in the images. **Boxed areas** are enlarged below. **B:** Immunoblots for Parkin and phosphorylated Parkin (p-Parkin) using the mitochondrial fractions and whole cell lysates before and after CCCP treatment ($n = 5$). Parkin expression level was normalized to mitochondrial heat shock protein 70 (Mt-HSP70). The degree of phosphorylation was expressed as the ratio of phosphorylated Parkin after CCCP treatment to that prior treatment. **C:** Parkin mRNA level in Huh7 cells and JFH1-Huh7 cells before and after CCCP treatment ($n = 5$). The expression level for Parkin was normalized to GAPDH. **D:** Coimmunoprecipitation reveals more ubiquitinated Parkin in CCCP dose-dependent manner in Huh7 cells but not in JFH1-Huh7 cells. **E:** Immunoblots for Parkin using mitochondrial fractions of the livers or liver homogenates from non-TgM and TgM and from chimeric mice with or without HCV infection ($n = 5$ for each type of mouse). *$P < 0.05$.

CCCP specifically induces mitophagy in Huh7 cells and that the HCV infection has an inhibitory effect on mitophagy in JFH1-Huh7 cells.

FL-N/35-transgenic mice and HCV-infected chimeric mice also showed reduced Parkin expression in the mitochondrial fraction of the liver with no change in Parkin expression levels in whole liver homogenates (Figure 2E). Serum human albumin levels, which serve as useful markers for the extent of replacement with human hepatocytes, were 16.0 ± 7.2 mg/mL in chimeric mice with HCV infection and 11.9 ± 1.7 mg/mL in chimeric mice without HCV infection (Figure 3A). These findings suggest that there was
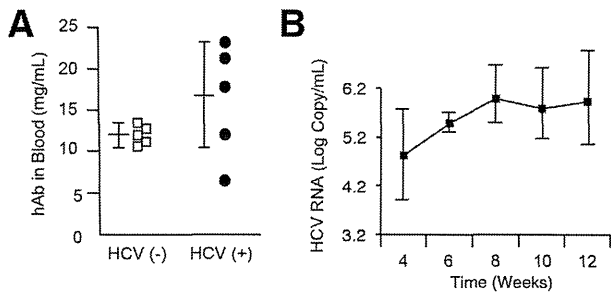
Figure 3 Human albumin and HCV RNA levels in the serum of chimeric mice with or without HCV infection. **A:** Human albumin (hAb) levels in the serum of 3-month-old chimeric mice with or without HCV infection. **B:** Serial change in HCV RNA levels in the serum after HCV infection in chimeric mice ($n = 5$).

a replacement index of >90% according to a graph of the correlation between these two parameters identified in a previous study.[25] Moreover, serum HCV RNA levels increased after infection with HCV (Figure 3B). HCV infection also suppressed the translocation of Parkin to the mitochondria in human hepatocytes.

Interaction between Parkin and the HCV Core Protein

A loss of $\Delta\Psi$ stabilizes the mitochondrial accumulation of PINK1, and PINK1 recruits Parkin from the cytoplasm to depolarized mitochondria via its kinase activity.[13–15] We confirmed that Parkin was phosphorylated to the same degree after CCCP treatment regardless of HCV infection. Therefore, we next examined the mitochondrial accumulation of PINK1. Our results indicate that PINK1 accumulated in the mitochondrial fraction after CCCP treatment, and PINK1 expression levels in whole cell lysates were comparable irrespective of HCV infection (Figure 4A). In

addition, blocking PINK1 protein expression with siRNA (Figure 4B) strikingly suppressed Parkin phosphorylation (Figure 4C) and the mitochondrial Parkin signal after CCCP treatment in Huh7 cells (Figure 4D), indicating that PINK1 recruits Parkin from the cytoplasm to depolarized mitochondria via its kinase activity. Suppressed translocation of Parkin to the mitochondria by HCV infection was also confirmed after treatment with valinomycin, a K^+ ionophore that rapidly dissipates $\Delta\Psi^{32}$ (Figure 4E).

We next examined the association between HCV protein and Parkin and hypothesized that HCV proteins may suppress Parkin translocation to the mitochondria. Coimmunoprecipitation experiments revealed that Parkin associated with the HCV core protein but not other HCV proteins, such as NS3, NS4A, and NS5A, regardless of CCCP treatment (Figure 5A). These results suggest that the HCV core protein specifically suppressed Parkin translocation to impaired mitochondria by interacting with Parkin.

Finally, we investigated which specific Parkin domain is critical for the interaction with the HCV core protein. The proposed Parkin architecture consists of an N-terminal ubiquitin-like domain, a really interesting new gene (RING) 0 domain (RING0), and a C-terminal in-between RING domain[33] (Figure 5B). Of these domains, the RING0 domain and a complete carboxy-terminal RING configuration are critical for the translocation of Parkin to damaged mitochondria and for consequent mitophagy.[13] By using the HCV core protein as bait and either an N-terminal fragment of Parkin, including RING0 (designated Parkin 1 to 215), or a C-terminal fragment of Parkin, not including RING0 (designated Parkin 216 to 465) as prey, a Yeast Two-Hybrid assay identified a specific interaction between Parkin 1 to 215 and the HCV core protein, which was visualized as a strong blue color (activation of the *MEL1* gene encoding
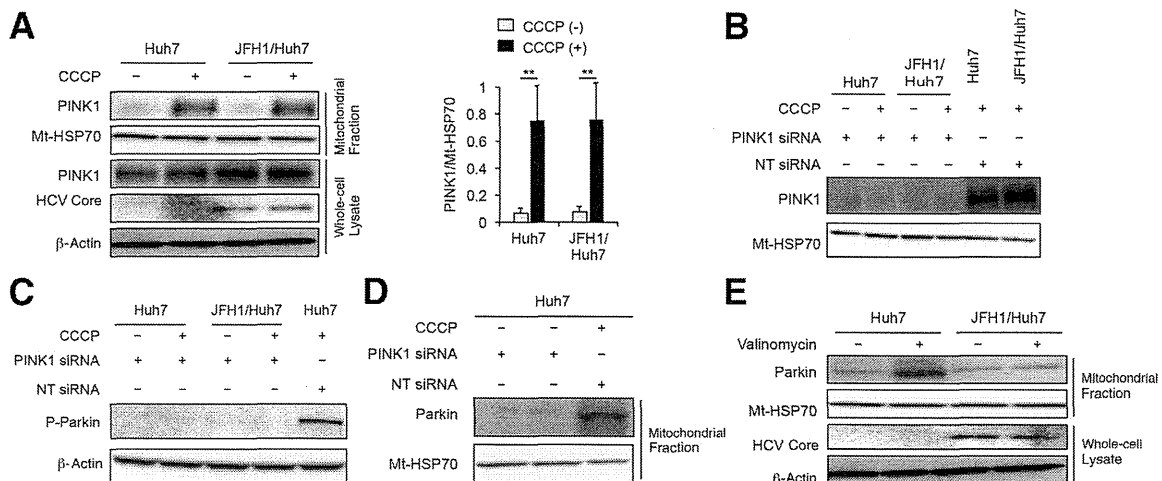

Figure 4 Mitochondrial accumulation of PINK1 after carbonyl cyanide *m*-chlorophenylhydrazone (CCCP) treatment and effect of PINK1 silencing on phosphorylation and mitochondrial translocation of Parkin. **A:** Immunoblots for PINK1 using mitochondrial fractions or whole cell lysates of Huh7 and JFH1-Huh7 cells before and after CCCP treatment ($n = 5$). Immunoblots for PINK1 using mitochondrial fractions (**B**), for phosphorylated Parkin (P-Parkin) using whole cell lysates (**C**), and for Parkin using mitochondrial fractions (**D**) of Huh7 and/or JFH1-Huh7 cells before and after CCCP treatment with or without an siRNA-mediated blockade of PINK1 expression. **E:** Immunoblots for Parkin using the mitochondrial fractions of Huh7 and JFH1-Huh7 cells before and after a 3-hour valinomycin treatment. **$P < 0.01$. Mt-HSP70, mitochondrial heat shock protein 70; NT siRNA, nontargeting siRNA.

– 471 –
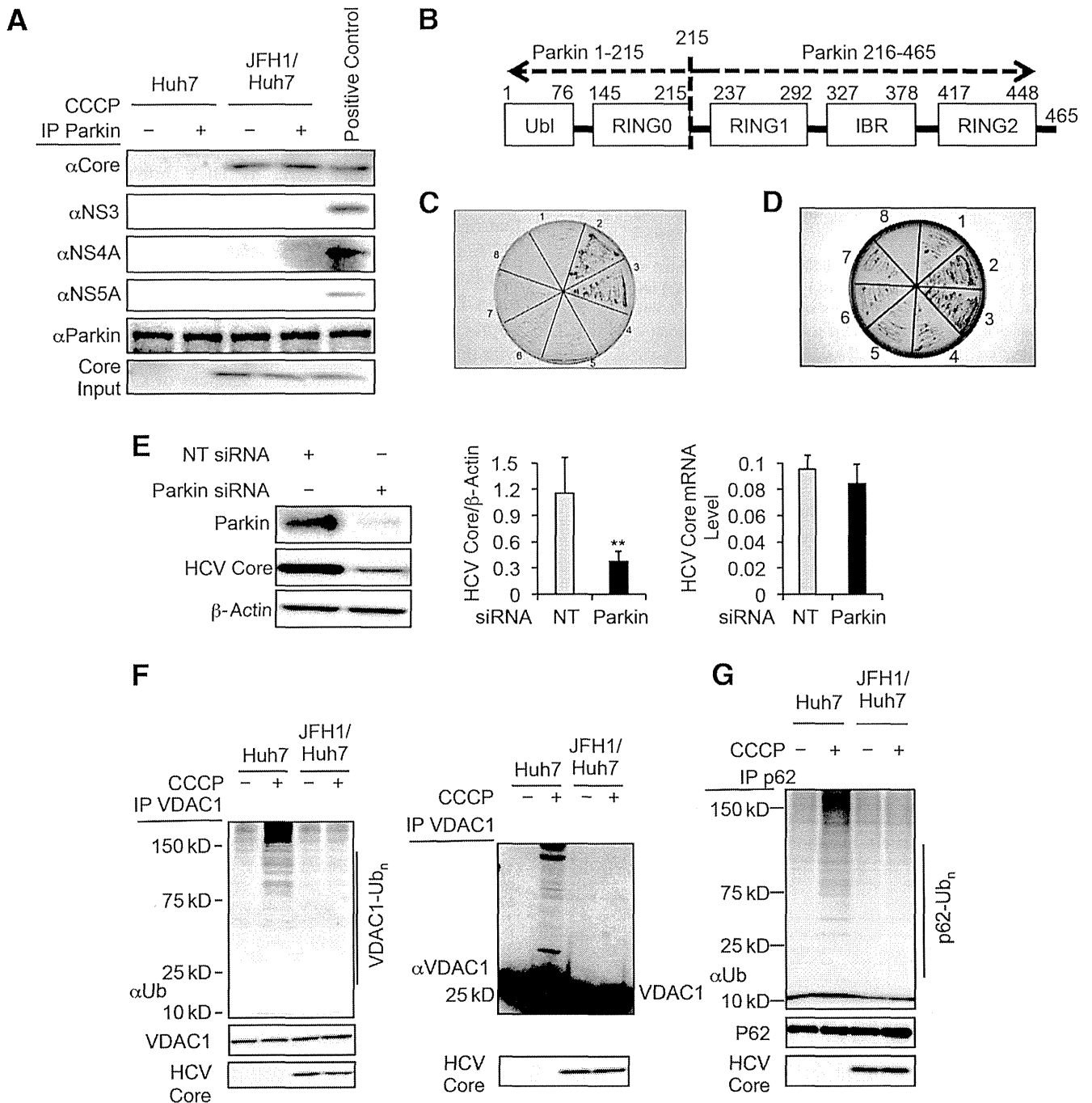
Figure 5 Interaction between Parkin and HCV core protein, effect of Parkin silencing on HCV replication, and reduction of mitochondrial outer membrane ubiquitination. **A:** Coimmunoprecipitation reveals a specific interaction of Parkin with the HCV core protein. **B:** The proposed Parkin architecture and a schematic diagram of Parkin domains. **C** and **D:** A Yeast Two-Hybrid assay identifies a specific interaction between Parkin 1 to 215 and the HCV core protein. The bait and prey for each section (1 to 8) in **C** are as follows: 1, none and none; 2, p53 and large T antigen (positive control); 3, HCV core and Parkin 1 to 215; 4, HCV core and Parkin 216 to 465; 5, HCV core and none; 6, none and Parkin 1 to 215; 7, none and Parkin 216 to 465; 8, no yeast. The bait and prey for each section in **C** were reversed in **D**. **E:** The HCV core protein and HCV core mRNA levels in JFH1-Huh7 cells with or without an siRNA-mediated blockade of Parkin expression ($n = 5$). **F:** Coimmunoprecipitation reveals more VDAC1 ubiquitination in Huh7 cells after carbonyl cyanide m-chlorophenylhydrazone (CCCP) treatment. Various sizes of VDAC1 immunoprecipitates are also detected by immunoblotting using an anti-VDAC1 antibody in Huh7 cells after CCCP treatment. **G:** Coimmunoprecipitation reveals more p62 ubiquitination in Huh7 cells after CCCP treatment. $**P < 0.01$. IBR, in-between RING; NT, nontargeting siRNA; Parkin, Parkin-targeting siRNA; Ubl, ubiquitin-like.

α-galactosidase) (Figure 5C). In contrast, Parkin 216 to 465 did not interact with the HCV core protein. The same results were found when the core protein was used as prey and different domains of Parkin were used as bait (Figure 5D),

indicating that this interaction between the two proteins was nonpolar. A previous mutational analysis of Parkin revealed that soluble Parkin mutants K211N, T240R, and G430D do not translocate to the mitochondria.[13] Although we have not
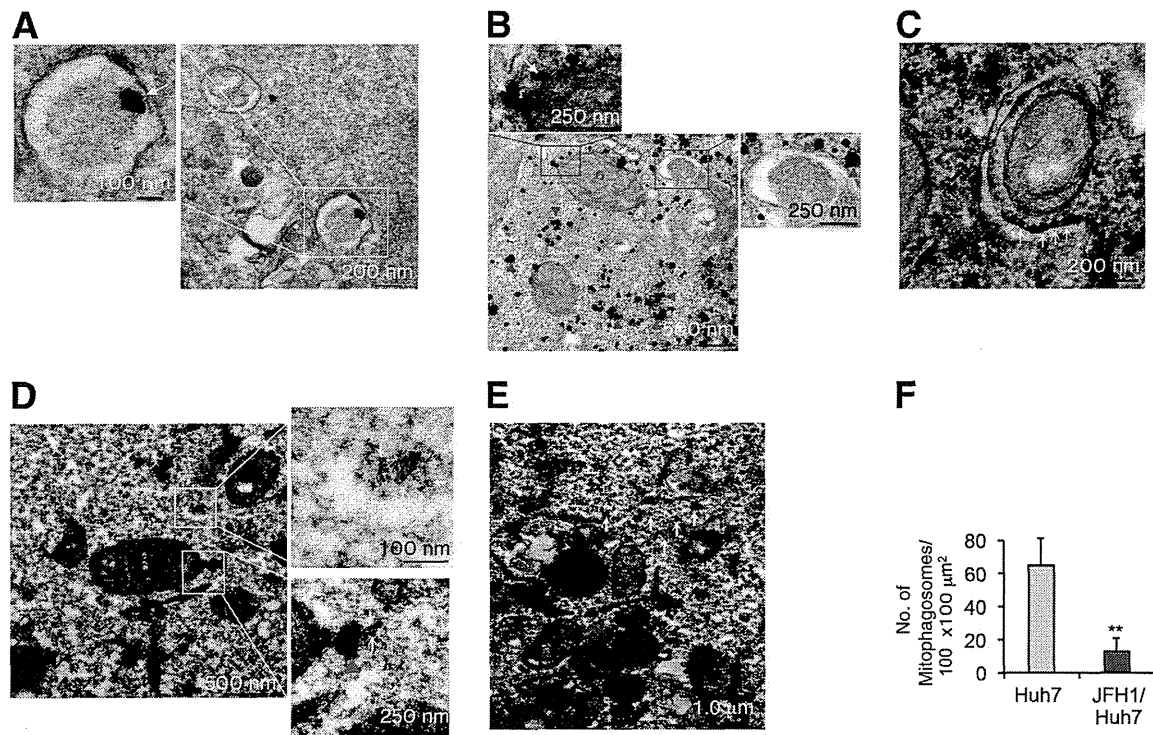
Figure 6 Electron microscopy of Huh7 cells and JFH1-Huh7 cells after carbonyl cyanide m-chlorophenylhydrazone (CCCP) treatment. **A–E:** Electron micrographs. **Boxed areas** are enlarged on left (Huh7 cell; **A**), above and on the right (Huh7 cell; **B**), and on the right (JFH1-Huh7 cell; **D**). The **arrows** indicate Parkin labeled with gold on the mitochondrial outer membrane (**A** and **B**), LC3 protein labeled with diaminobenzidine (DAB) on elongating isolation membrane that sequesters a single mitochondrion (Huh7 cells; **C**), Parkin core (**D**), and Parkin labeled with gold (JFH1-Huh7 cell; **E**). The **arrowheads** indicate Parkin labeled with gold (**B**) and HCV core (**D**). **F:** The number of mitophagosomes per 100 × 100 µm^2 was calculated for four randomly selected views. **$P < 0.01$.

determined whether the HCV core protein binds to the region that includes lysine (K) 211 in the RING0 domain, the specific interaction of Parkin 1 to 215 with the HCV core protein raises the possibility that the core protein inhibits Parkin translocation to the mitochondria by affecting lysine 211.

After we confirmed the specific interaction between the HCV core protein and Parkin, we investigated whether Parkin affects HCV replication to investigate the functional role of the interaction between both proteins in the HCV infectious process. Parkin silencing significantly inhibited HCV replication, as indicated by a decrease in HCV core protein expression, but did not affect HCV core mRNA levels (Figure 5E). These results suggest that the association of the HCV core protein with Parkin plays a functional role in HCV propagation, although further studies are required to clarify the mechanisms.

Suppressed Ubiquitination of the Mitochondrial Outer Membrane Protein VDAC1

The next step in mitophagy after Parkin translocation to the mitochondria is the ubiquitination of mitochondrial outer membrane proteins.[13,16] Coimmunoprecipitation experiments revealed that various sizes of ubiquitinated VDAC1 species in the mitochondrial outer membrane[13] were present after CCCP treatment in Huh7 cells but not in JFH1-Huh7

cells (Figure 5F). Western blot analysis of VDAC1 immunoprecipitates revealed various sizes of VDAC1 species after CCCP treatment in Huh7 cells but not in JFH1-Huh7 cells (Figure 5F). The autophagic adaptor p62 aggregates ubiquitinated proteins by polymerizing with other p62 molecules.[13] Similarly, coimmunoprecipitation experiments revealed that CCCP treatment induced various sizes of ubiquitinated p62 species in Huh7 cells but not in JFH1-Huh7 cells (Figure 5G). These results suggest that HCV infection inhibited the Parkin-induced ubiquitination of the depolarized mitochondria.

Suppressed Mitophagosome Formation

During mitophagy, the isolation membrane sequesters a single mitochondrion or a cluster of mitochondria to form an autophagosome (mitophagosome). A single mitochondrion with Parkin on its outer membrane was sequestered by the isolation membrane after CCCP treatment in Huh7 cells (Figure 6A). Parkin in close proximity to the mitochondria and association of Parkin with mitochondrial outer membrane were observed more frequently in Huh7 cells than in JFH1-Huh7 cells (Figure 6, B, D, and E). In addition, LC3 was present on elongating isolation membrane that sequesters a single mitochondrion after CCCP treatment in Huh7 cells (Figure 6C). The number of mitophagosomes, calculated as the number of autophagosomes that contain